frontiers in Materials

ORIGINAL RESEARCH
published: 14 May 2021
doi: 10.3389/fmats.2021.651970

Effects of Titanium Corrosion Products on *In Vivo* Biological Response: A Basis for the Understanding of Osseointegration Failures Mechanisms

Claudia Cristina Biguetti[1,2], *Franco Cavalla*[1], *Angélica Cristina Fonseca*[1], *Andre Petenucci Tabanez*[1], *Danyal A. Siddiqui*[2], *Sutton E. Wheelis*[2], *Rumio Taga*[1], *Walid D. Fakhouri*[3], *Renato Menezes Silva*[3], *Danieli C. Rodrigues*[2] and *Gustavo Pompermaier Garlet*[1]*

[1]Department of Biological Sciences, Bauru School of Dentistry, Universidade de São Paulo, Bauru, Bauru, Brazil, [2]Department of Bioengineering, University of Texas at Dallas, Richardson, TX, United States, [3]Center for Craniofacial Research, School of Dentistry, University of Texas Health Science Center at Houston, Houston, TX, United States

OPEN ACCESS

Edited by:
Abdul Samad Khan,
Imam Abdulrahman Bin Faisal University, Saudi Arabia

Reviewed by:
Omar Omar,
Imam Abdulrahman Bin Faisal University, Saudi Arabia
Lia Rimondini,
University of Eastern Piedmont, Italy

***Correspondence:**
Gustavo Pompermaier Garlet
garletgp@usp.br

Specialty section:
This article was submitted to Biomaterials, a section of the journal Frontiers in Materials

Received: 01 February 2021
Accepted: 26 April 2021
Published: 14 May 2021

Citation:
Biguetti CC, Cavalla F, Fonseca AC, Tabanez AP, Siddiqui DA, Wheelis SE, Taga R, Fakhouri WD, Silva RM, Rodrigues DC and Garlet GP (2021) Effects of Titanium Corrosion Products on In Vivo Biological Response: A Basis for the Understanding of Osseointegration Failures Mechanisms. Front. Mater. 8:651970. doi: 10.3389/fmats.2021.651970

Corrosion resistance is a key feature of titanium biocompatibility. However, Ti surfaces exposed to critical environments (such as, chronic infection and inflammation) can undergo corrosion processes *in vivo*, leading to an unfavorable biological response and clinical failure, which remains poorly explored. In this study, we characterized an experimental model to replicate the surface features of Ti corrosion process observed within *in vivo* failures, and the cellular, tissue and molecular events associated with corroded Ti surface implantation into subcutaneous and bone tissue of C57Bl/6 mice. Prior to *in vivo* implantation, commercially pure Ti Commercially pure titanium and Ti–6Al–4V alloy (Ti64) specimens were exposed to electrochemical polarization in 30% citric acid, while being polarized at 9 V against a saturated calomel electrode for 20 min. The electrochemical attack induced accelerated corrosion on both Ti-based specimens, producing structural and chemical changes on the surface, comparable to changes observed in failed implants. Then, microscopy and molecular parameters for healing and inflammation were investigated following control and corroded Ti implantation in subcutaneous (cpTi disks) and oral osseointegration (Ti64 screws) models at 3, 7, 14 and 21 days. The host response was comparatively evaluated between control and corroded Ti groups by microCT (bone), histology (H&E, histomorphometry, immunostaining and picrosirius red), and real-time PCR array for inflammatory and healings markers. Corroded cpTi disks and Ti64 screws induced a strong foreign body response (FBR) from 3 to 21 days-post implantation, with unremitting chronic inflammatory reaction lasting up to 21 days in both subcutaneous and osseointegration models. In the subcutaneous model, FBR was accompanied by increased amount of blood vessels and their molecular markers, as well as increased TRAP+ foreign body giant cell count. In the osseointegration model, failures were identified by an osteolytic reaction/bone loss detected by microCT and histological analyses. The corroded devices were associated

with a dominant M1-type response, while controls showed transient inflammation, an M2-type response, and suitable healing and osseointegration. In conclusion, corrosion of Ti-based biomaterials induced exacerbated inflammatory response in both connective tissue and bone, linked to the upregulation of fibrosis, pro-inflammatory and osteoclastic markers and resulted in unfavorable healing and osseointegration outcomes.

Keywords: titanium, osseointegration, failure, inflammation, mice, electrochemical corrosion

INTRODUCTION

Materials comprised of titanium (Ti), especially commercially pure Ti (cpTi) and Ti-6aluminum–4vanadium alloy (Ti64), are widely used for biomedical applications due to their biocompatibility (Flatebø et al., 2006; Hanawa, 2019; Dini et al., 2020), favorable mechanical properties (Flatebø et al., 2006; Niinomi, 2008; Niinomi et al., 2016) and corrosion resistance (Shah et al., 2016; Hanawa, 2019). Ti-based implant biomaterials are usually the material of choice in oral implantology and orthopedics due to its ability to osseointegrate (Davies, 2003; Flatebø et al., 2006; Mouhyi et al., 2012). Particularly, cpTi is mostly used to manufacture the implant body of dental fixtures, while Ti64 alloy is commonly used for the healing abutment and prosthetic parts (Noronha Oliveira et al., 2018) and orthopedic implants (Arteaga et al., 2021). Corrosion resistance is a predominant and necessary feature for cpTi and Ti6Al4V biocompatibility with hard and soft tissues (Hanawa, 2019). Among other metals and alloys used in dentistry, Ti-based biomaterials have the highest redox potential in the presence of *in vivo* electrochemical factors within acidic and saline environments (enzymes, acids, bases, organic molecules), resulting in greater corrosion resistance (Mouhyi et al., 2012; Noumbissi et al., 2019). Specifically, the corrosion resistance of this biomaterial stems from its capability to spontaneously form a native titanium dioxide layer (TiO_2) when exposed to air and aqueous environments, such as blood and/or saliva (Lausmaa and Linder, 1988). The natural oxide layer formed at the Ti-based biomaterial and host interface immediately following implantation may persist long-term, serving as a protective barrier to continued metal ion release into the surrounding environment (Tengvall and Lundström, 1992; Okazaki and Gotoh, 2005), ultimately mitigating adverse tissue reactions (Asri et al., 2017).

Under ideal biological conditions (e.g., no previous infection, healthy implant host), the initial trauma and inflammatory response following Ti-based device implantation results in the release and formation of a host protein layer on the oxide surface (Albertini et al., 2015). The interaction of these proteins with the Ti-based biomaterial surface seems to be beneficial and essential to trigger the first events of implant osseointegration (Albertini et al., 2015; Biguetti et al., 2019). This initial inflammatory response has been reported to be transient and moderate, as shown in histological and molecular analysis of samples from oral osseointegration of Ti64 screws in a mouse model (Mouraret et al., 2014; Biguetti et al., 2018). This event is characterized by an elevated expression of tissue healing/regeneration, bone cell differentiation, mesenchymal stem cells (MSCs) and M2 macrophage markers at implantation sites (Biguetti et al., 2018; Biguetti et al., 2019). Therefore, under ideal conditions, a transitory and controlled inflammatory immune response results in a constructive scenario that supports the gradual bone deposition and maturation surrounding Ti-based implants (Biguetti et al., 2018).

Conversely, products from oral bacterial biofilms and/or chronic inflammatory environments present detrimental effects to both Ti-based devices (implant and its prosthetic parts) and host cells/tissues (Messer et al., 2009; Mouhyi et al., 2012; Penmetsa et al., 2017; Delgado-Ruiz and Romanos, 2018; Noumbissi et al., 2019; Dini et al., 2020). Experimental studies show that a chronic inflammatory milieu, involving the sustained release of pro-inflammatory mediators and/or altered cell function, generates an electrochemical environment that can negatively affect the Ti-based biomaterials, initiating a corrosion process and ion dissolution (Messer et al., 2009; Messer et al., 2010; Mouhyi et al., 2012). By definition, corrosion consists of metallic material degradation induced by chemical or electrochemical events (Delgado-Ruiz and Romanos, 2018; Dini et al., 2020) and leads to a gradual loss of metallic ions from the biomaterial surface to the surrounding environment (Saini et al., 2015; Asri et al., 2017). Indeed, several studies have shown that even cpTi and Ti64 can be susceptible to corrosion under challenging *in vivo* and *in vitro* conditions in dentistry and orthopedics (Mouhyi et al., 2012; Shah et al., 2016; Wheelis et al., 2016; Noronha Oliveira et al., 2018; Arteaga et al., 2021). When Ti implants are exposed to an electrochemical attack, the corrosion process can initiate metal ion dissolution from the biomaterial surface leading to its accumulation within the surrounding tissue (Sridhar et al., 2016). Indeed, numerous histopathological studies with clinical samples suggest a positive association between the inflammatory response in peri-implant mucosa and the presence of corrosion products from cpTi and Ti64 in sample biopsies (Olmedo et al., 2004; Flatebø et al., 2006; Olmedo et al., 2012; Penmetsa et al., 2017; Soler et al., 2020). It is suggested that when the oxide layer is exposed to an aggressive inflammatory environment, Ti corrosion resistance becomes significantly altered, disrupting the maintenance of osseointegration over time, as well limiting the possibility of Ti surface re-integration with surrounding bone (Mouhyi et al., 2012; Rodrigues et al., 2013; Arteaga et al., 2021). Several studies in the literature also show that, in addition to host and bacterial acidic factors, commercial therapeutic formulations used for detoxification and/or treatment purposes can also initiate corrosion of Ti and its alloys (Souza et al., 2015; Wheelis

et al., 2016; Mombelli et al., 2018; Noronha Oliveira et al., 2018; Lakkasetter Chandrashekar et al., 2021). For example, *in vitro* studies suggest that certain chemical agents used in dentistry [i.e., citric acid doxycycline (50%), tetracycline, chlorhexidine (0.12, 1%)] are able to erode the oxide layer, cause morphological changes on the biomaterial surface and initiate a corrosion process on cpTi or Ti64 (Wheelis et al., 2016; Ramesh et al., 2017). In clinical studies, a positive association exists between electrochemical attack, Ti corrosion and biological complications. However, the cause-and-effect relationship between Ti corrosion and loss of osseointegration remains to be addressed for in-depth clinical and preclinical research. (Mouhyi et al., 2012; Mombelli et al., 2018; Soler et al., 2020).

From a biological point of view, the corrosion of Ti-based biomaterials potentially mediated by acidic products created from chronic inflammation and consequent metal ion dissolution, may create a feedback loop that exacerbates inflammation leading to a destructive tissue response as is the case with already integrated orthopedics and dental implants (Mouhyi et al., 2012; Sridhar et al., 2016; Rodrigues et al., 2013; Pettersson et al., 2017). A destructive response culminating in decreased bone-implant contact has also been observed during the initial stages of osseointegration, particularly after implanting artificially corroded Ti implants in rat tibia (Olmedo et al., 2008). In this animal model, corrosion products were observed surrounding blood vessels and inside macrophages (Olmedo et al., 2008). A histopathological study from Olmedo et al. (2012) evaluated the presence of metal particles and inflammatory reaction in 153 human peri-implant mucosa biopsies in proximity to cpTi or Ti64 cover screws of Ti implants (Olmedo et al., 2012). All patients were healthy, presented optimal oral hygiene, and had no signs of peri-implant bone loss. However, 41% of the biopsies presented metal particles associated with macrophages and T lymphocytes, indicating an initial immunological response in the supra-implant mucosa (Olmedo et al., 2012). A recent study with 44 patient subjects indicated that Ti dissolution from dental implants was associated epigenetic regulation at peri-implant sites (DNA hypermethylation), which could be related to changes in immune response during peri-implant disease (Daubert et al., 2019). A comprehensive literature review combining data from 17 studies related to the dissemination and effects of released ions and particles on peri-implant tissues shows that: (i) metal ions and particles can be found in local tissues (peri-implant bone and vessels) and distant sites (liver, spleen and lymph nodes); (ii) corrosion products released after implant decontamination are associated with chronic inflammation; (iii) the presence of nanoparticles leads to greater cytotoxic effects than larger particles; and (iv) other metal particles from released from Ti64 biomaterials (i.e. V and Al) are also cytotoxic and can lead to cell death (Noronha Oliveira et al., 2018). Ti particles may also differently affect the macrophage polarization state, as well the activity of M1 and M2 macrophages in inflammatory osteolytic response. An *in vitro* study showed that Ti particles in general enhance M1 macrophage response at transcriptome and proteome levels, with increased production mediators involved with inflammation and aseptic osteolysis (i.e., TNF alpha, IL1b, CCL2, IL6) (Pajarinen et al., 2013). On the other hand, M2 macrophages in contact with Ti particles presented a decrease in IL10 production (Pajarinen et al., 2013). However, the *in vivo* pathological and molecular events involved in the destructive inflammation to corroded Ti-based devices remains under-recognized.

As previously demonstrated, *in situ* degradation of a Ti-based biomaterials is not just detrimental because it alters the structural integrity of the implant but also because it can potentially/allegedly trigger a pathological response leading to early and/or late failure of osseointegration. Therefore, the aim of the present study was to elucidate the biological effects of Ti corrosion on osseointegration. In this study, we characterized an experimental model to replicate the surface features of Ti corrosion process observed for *in vivo* failures, based on the electrochemical polarization-induced surface damage of Ti-based devices and characterized the biological response (cellular, tissue and molecular events) to corroded cpTi and Ti64 implantation into subcutaneous and bone tissue of C57Bl/6 mice.

MATERIALS AND METHODS

Materials and Corrosion Protocols

Commercially pure titanium (cpTi) disks (6 mm Ø and 1.5 mm thickness) and Ti alloy screws (titanium-6 aluminum-4 vanadium alloy, NTI-Kahla GmbH Rotary Dental Instruments, Kahla, Ø 0.6 and 4 mm in length), designated here as Ti64, were used for this study. Both, cpTi disks and Ti64 screws were corroded by electrochemical polarization and compared to control samples (samples with no treatment). Per previous studies demonstrating the detrimental effect of citric acid exposure to Ti corrosion behavior, electrochemical polarization was used to directly induce corrosion damage by immersing cpTi disks and Ti64 screws in 30% citric acid (% w/v) in deionized water (Thermo-Fisher Scientific) (pH ≈ 2) while being polarized at 9 V against a saturated calomel electrode (SCE) for 20 min (Wheelis et al., 2016; Rodrigues et al., 2013; Ramesh et al., 2017). Prior to further characterization, control and corroded samples were cleaned by ultrasonication with sequential immersion in acetone, deionized water, and ethanol.

Surface Morphology of cpTi Disk and Ti64 Screw

Multiple areas of one representative control and corroded cpTi disk and Ti64 screw were observed using an optical microscope (VHX-2000 Digital Microscope, Keyence). The surface morphology of the specimens was evaluated, and characteristic features of control and treated specimens were noted, following previous analysis described for corroded dental implants retrieved due to late failure (Rodrigues et al., 2013).

Corrosion Testing

Before electrochemical testing, one cpTi disk or Ti64 screw alloy as received after electrochemical polarization were prepared by mounting them with alligator clips. Electrical tape and two layers of a commercial insulation coating (MiccroStop, Tolber Chemical

Division) were then partially applied over the specimens and alligator clip to isolate and only expose the desired specimen surface area to the electrolyte. Electrochemical testing to predict the corrosion behavior of control and treated specimens was performed based on guidelines established in ASTM F2129-15. A standard three-electrode electrochemical cell was connected to a potentiostat (Interface 1000, Gamry Instruments) using a SCE as the reference electrode and a graphite rod as the counter electrode. Open-circuit potential (OCP) measurements were monitored for 1 h to allow for equilibrium to be reached in 1X phosphate buffered saline (PBS) at 37°C. The OCP value after 1 h was recorded as the sample's corrosion potential, E_{corr}. Afterward, specimens underwent linear polarization resistance measurements by polarizing the specimen from −10 to 10 mV vs. E_{corr} at a scan rate of 0.1667 mV/s in order to measure the polarization resistance (Rp). Finally, anodic Tafel polarization was performed by polarizing the specimen from E_{corr} to 250 mV above E_{corr} at a scan rate of 1 mV/s. Based on the anodic Tafel curve, the corrosion current density (i_{corr}) was extrapolated to calculate the corrosion rate using equations specified in ASTM G102-89.

Surface Characterization by X-Ray Photoelectron Spectroscopy

The chemical composition of control and corroded cpTi disks was assessed using a PHI 5000 Versa Probe II X-ray Photoelectron Spectrometer equipped with an ion gun to allow for depth profiling by sputtering with an argon source (1 kV). XPS measurements were taken at a 45° angle to the surface using an Al Kα source (1486.6 eV) with the vacuum chamber maintained below 10^{-8} Torr. To compare the relative thickness of the oxide layers on control and corroded specimens, the surface elemental composition was determined for the as cleaned surface, after sputtering for 1 min, and after sputtering for an additional minute (2 min in total). The survey scan was performed using a pass energy of 187.50 eV with a 0.8 eV step size while higher resolution elemental scans were obtained using a 23.5 eV pass energy with a 0.2 eV step size. Two points on each specimen were analyzed to ensure homogeneity of the chemical environment across the specimen surface, with the exception of the implant screws, which could not be analyzed due to specimen geometry and dimensions making detection by XPS impractical. The XPS spectra's energy calibration was performed by setting the C1s peak associated with adventitious carbon to 285.0 eV. All XPS data analysis was performed using Casa XPS 2.3.17 software.

Animals and Experimental Design

All animal procedures were submitted and approved by the local Institutional Committee for Animal Care and Use (CEEPA-FOB/USP, #012/2014) and according to recommendations in the Guide for the Care and Use of Laboratory Animals of the National Institutes of Health (Institute of Laboratory Animal Resources (U.S.), 2011). Forty male C57Bl/6 mice (10-weeks-old, 25 g of weight in average) were used for subcutaneous cpTi implantation in left and right site of animal dorsa, each side being used for one type of analysis (microscopic or molecular), with 20 mice used for each group (control or corroded). Eighty C57Bl/6 male mice (10-weeks-old, 2 5 g of weight in average) were used for Ti64 oral osseointegration model (48 for microscopic and 32 for molecular analysis). While cpTi disks were used for subcutaneous implantation, Ti64 screws were used for bone implantation in an oral osseointegration model, as previously described (Biguetti et al., 2019). Both cpTi disk subcutaneous implantation and Ti64 screw osseointegration model were analyzed at 3, 7, 14, and 21 days post Ti-implantation for all analysis. Experimental groups for subcutaneous implantation were designed such that a cpTi disk on the left side was used for microscopy and a cpTi disk from the same group in the right side was used for molecular analysis. Then, 5 biological replicates per group/time point were selected for microscopic analysis (histological and histomorphometric analysis, birefringence, immunohistochemistry and immunofluorescence), and 5 biological replicates, from the same animals, were used for molecular assays to measure the RNA expression level. Experimental groups for the oral osseointegration model received only one screw in the right side of the maxillary bone. Groups (control or corroded) were comprised of 10 animals per time point but with 6 animals per group/time point for microscopic analysis (microCT, histological and histomorphometric analysis and birefringence) and 4 animals for molecular assays using real-time PCR (RT-PCR). For both types of surgical procedures, cpTi disk and Ti64 screw implantation, C57Bl/6 mice were administrated with general sedation by using ketamine chloride 80 mg/kg (Dopalen, Agribrands Brasil) and xylazine chloride 160 mg/kg (Anasedan, Agribrands Brasil). No antibiotics and anti-inflammatory substances were given to the animals, to avoid interferences on targeted immunological pathways.

Surgical Protocols for Ti-Based Devices Implantation and Sample Collection

Prior to implantation, corroded samples (cpTi disks and Ti64 screws) were successively washed in deionized water, 70% ethanol and acetone and then dried. All samples (control and corroded specimens) were sterilized by autoclaving before surgical procedures, as previously described (Noumbissi et al., 2019). Oral Ti64 screw implantation and subcutaneous cpTi disk implantation were performed as previously described (Biguetti et al., 2019). In brief, both surgeries were performed after general sedation. For cpTi subcutaneous implantation, mice received local anesthesia by injection of bupivacaine at the site of incision before surgery to reduce pain, and longitudinal incisions were made at either side of the dorsal midline, where a subcutaneous pocket for each fragment was prepared by gentle dissection. On the left side, the animal received the cpTi disk for microscopic analysis, whereas on the right side, a cpTi disk from the same group (control or corroded) was used for molecular analysis. Incisions were sutured, and mice were kept in a cage placed on a heated pad for 2 h for post-op recovery. For oral implantation, Ti64 screw was placed in the right side of the edentulous alveolar crest of the maxilla. A previous guide perforation was made in bone by using a Ø 0.50 mm pilot drill (NTI-Kahla GmbH Rotary Dental Instruments, Kahla), and the implant was screwed down in the bone using a Castroviejo micro needle holder (Fine Science Tools). Mice were provided with sterile

standard solid mouse chow during all experimental periods of this study, except throughout the first 72 h post-Ti implantation for oral osseointegration model, in which diet was crumbled. At the end of experimental periods, mice were euthanized, and subcutaneous tissue surrounding the cpTi disks and the Ti64 screws in maxillary samples were removed for microscopic and/or molecular analysis. The subcutaneous and bone samples selected for microscopic analysis were fixed in PBS-buffered formalin (4%) solution for 48 h at room temperature with the devices (disks or screws) in place, washed overnight in running water and processed for paraffin inclusion, with the exception of maxillae, which were maintained in 70% fixative alcohol until the completion of the microCT scanning. After microCT scanning, bone specimens were decalcified in 4.13% EDTA (pH 7.2) following histological processing protocols. Samples for molecular analysis were stored in RNAlater with the devices (disks and screws) in place and kept at −80°C until the molecular assays (Ambion). After samples were homogenized for molecular assays, the cpTi or Ti64 devices were removed, and RT-PCR array reactions were performed according to a previous study (Vieira et al., 2015).

Micro-Computed Tomography (MicroCT) Assessment

Osseointegration sites of mice maxillae were scanned and analyzed as previously described (Noumbissi et al., 2019). Scans from maxillae containing the Ti implants were obtained by using Skyscan 1176 System (Bruker Microct) at 80 kV, 300 μA, 180° of rotation and exposure range of 1°. Image projections were subsequently processed in the NRecon software (Bruker Microct), and quantitative evaluation of bone formation at the implant interface was assessed using CTAn 1.1.4.1 software (Bruker Microct). Three-dimensional images were obtained by CT-Vox 2.3 software. Bone volume proportion (BV/TV, %) was used as the parameter of bone quantification at the Ti64 surface and bone interface area. The region of interest (ROI) included a diameter of 700 μm and length of 500 μm.

Sample Processing for Microscopic Assays

Subcutaneous and bone specimens containing the biomaterials (control and corroded Ti-based devices) were fixed in 4% paraformaldehyde. For histological analysis, the Ti64 screw was carefully removed after complete bone decalcification, by using the same micro needle holder used for its insertion. For subcutaneous samples, cpTi disks were removed after fixation and before paraffin inclusion. Then, bone and/or subcutaneous tissues surrounding the implant sites were embedded in paraffin for sectioning at 5 μm of thickness. For subcutaneous disk implantation, a total of five samples (biological replicates) and eight semi-serial sections (technical replicates) were considered for histomorphometry with sections stained with hematoxylin-eosin (H&E), while four semi-serial sections were considered for birefringence and four semi-serial sections for immunodetection (immunohistochemistry or immunofluorescence). For the oral osseointegration model, a total of six samples (biological replicates) and nine semi-serial sections (technical replicates) from the central region of implantation sites in the maxilla were taken for H&E histomorphometry while four semi-serial sections were taken for birefringence analysis (Biguetti et al., 2018).

Histological, Histomorphometric Analysis (H&E) and Birefringence (Picrosirius Red)

H&E sections were used for histological description and histomorphometry, considering inflammatory and healing and/or foreign body reaction (FBR) parameters. Thus, the presence of residual blood clots, inflammatory cells, foreign body giant cells (FBGC), fibers, fibroblasts and blood vessels were analyzed in all semi-serial sections of subcutaneous and bone tissue. Additionally, osteoblasts (cuboid cells lining the bone matrix or osteoid), osteoclasts (multinucleated cells containing ruffled border and attached to the bone matrix), and bone matrix were also analyzed at sites of oral osseointegration. The descriptive analysis to distinguish cell types (i.e., FBGC vs. osteoclasts) and confirm histopathological events was performed by one calibrated examiner (CCB) and two experienced histologists (RT and GPG). A single calibrated investigator (CCB) performed all histomorphometric analysis according to a previous characterization study (Biguetti et al., 2018). Six histological fields were captured per each H&E section at ×100 magnification, comprising the region adjacent to thread spaces (for osseointegration) or disk space (for subcutaneous) and were under a 100 points grid in a quadrangular area, by using ImageJ software (Version 1.51, National Institutes of Health) (Biguetti et al., 2018; Biguetti et al., 2019). Points were quantified coinciding with the parameters of healing or FBR as previously cited (Biguetti et al., 2018; Biguetti et al., 2019). The same histological fields of osseointegration were assessed for bone to implant contact percentage (BIC %) at 21 days using ImageJ software (Version 1.51, National Institutes of Health). The length (μm) of the alveolar bone in direct contact with the Ti64 implant threads (spaces) was quantified as previously standardized in a similar model in Lewis rats (Wheelis et al., 2021). In brief, the entire implant length under the crest of maxillary bone was taken (implant length), followed by the length of the implant in contact with bone in the same field (bone contact). BIC % was analyzed by determining the percentage of bone contact relative to the implant length under the crest of maxillary bone. As a complementary approach, the collagen content was evaluated by birefringence analysis using picrosirius red staining. Also, for each subcutaneous or bone section, six histological fields were analyzed around the space of cpTi sample at ×40 magnification through polarizing lens coupled to a binocular inverted microscope (Leica DM IRB/E, Leica Microsystems Wetzlar GmbH) (Noumbissi et al., 2019). Images were captured with Leica Imaging Software (LAX, Leica Microsystems Wetzlar GmbH), and the quantification of birefringence brightness was performed using the AxioVision 4.8 software (Carl Zeiss Microscopy GmbH) considering the area in pixels of green, yellow and red spectra. All quantitative data were subject to statistical analysis. Results for histomorphometry and birefringence were presented as the mean area density for each structure considered in each examined group.

Immunolabeling Protocols for Subcutaneous Ti Implantation

Immunohistochemistry was performed for the detection of TRAP+ FBGCs, while immunofluorescence was performed for colocalization of inflammatory (M1) and regenerative (M2) macrophage markers. Immunohistochemistry or immunofluorescence protocols and labeled cells quantification was performed as previously described (Biguetti et al., 2018). For immunofluorescence, antigen retrieval was performed by boiling the histological slides in 10 mM sodium citrate buffer (pH 6) for 30 min at 100°C. Subsequently, the sections were permeabilized with 0.5% Triton X-100 in PBS and blocked with 1% bovine serum albumin diluted in 1x PBS for 1 h at room temperature. Then, sections were incubated with both primary antibodies: rabbit polyclonal anti-mouse CD80 (Abcam, ab64116) and goat polyclonal anti-mouse CD206 (ThermoFisher, #PA5-46994), both diluted at 1:100 in blocking solution and incubated overnight at 4°C. After repeated washing steps with PBS (3 times, 10 min each wash), sections were incubated with both secondary antibodies: Alexa Fluor®488 donkey anti-goat (Life Technologies, #A11055) and Alexa Fluor® 555 goat anti-rabbit (Life Technologies, #A21428). All secondary antibodies were diluted at 1:150 in blocking solution and incubated in a dark chamber for 2 h at room temperature. All sections were stained with DAPI (ThermoFisher, #D3571) and diluted at 3 μM in ddH2O for 10 min to visualize nuclei. Slides were mounted in with ProLong Gold Antifade Reagent (Invitrogen, P36930). Imaging was performed 48 h after mounting steps in a Nikon Eclipse Ni-U upright fluorescence microscope (Nikon instruments) equipped with a Zyla 5.5 sCMOS camera (Andor).

Gene Expression Patterns Along Tissue Repair on Corroded and Ti Control Surfaces

Samples containing the entire tissue containing implants from subcutaneous tissue and oral osseointegration sites were dissected using a stereomicroscope observing the same margins (1.5 mm of subcutaneous tissue from the disk margin and 2 mm of bone from the screw margin) from the implantation sites, in order to ensure minimal variability regarding the sample size. Samples were stored with the integrated Ti-based devices in RNA stabilization solution (RNAlater, Thermofisher, Waltham, MA, United States) until RT-PCR array reactions. Both implants (cpTi or Ti64) were removed after homogenizing the tissue samples for RNA extraction. RT-PCR array reactions were performed as previously described (Biguetti et al., 2018). Extraction of the total RNA from mouse tissues and complementary DNA synthesis were performed following methods previously described for oral osseointegration and subcutaneous implantation (Biguetti et al., 2019; Wheelis et al., 2021; Wheelis et al., 2020). The total RNA was extracted by using RNeasy kit (Qiagen Inc., Valencia, CA, United States), and the integrity of RNA samples was checked by 2100 Bioanalyzer (Agilent Technologies, Santa Clara, CA, United States). Synthesis of complementary DNA was performed by using 3 μg of RNA through a reverse transcription reaction (QuantiTectRTkit, Qiagen Inc., Valencia, CA, United States) (Vieira et al., 2015; Biguetti et al., 2018; Biguetti et al., 2019). Custom panels for "wound healing" (PAMM-121), "inflammatory cytokines and receptors" (PAMM-011) and "osteogenesis" (PAMM-026) (SABiosciences, Frederick, MD, United States) for gene expression profiling were implemented by using ViiA7 instrument (LifeTechnologies, Carlsbad, CA, United States). Data analysis was performed by using RT2 Profiler software (SABiosciences, Frederick, MD, United States) to normalize the initial geometric mean of three constitutive genes (GAPDH, ACTB, Hprt1), following normalization of the control group. Data were expressed as heat map fold change relative to the control group.

Statistical Analysis

Statistical tests were performed with GraphPad Prism 7.0 software (GraphPad Software Inc.). Data with normal distribution were analyzed using ANOVA followed by Bonferroni's multiple comparison post-hoc tests or student's *t*-test where applicable. For non-normal distributions, the Kruskal–Wallis test (followed by Dunn's test) and Mann–Whitney test were used. Values of $p < 0.05$ were considered statistically significant.

RESULTS

Surface Morphology of Ti Specimens

Images depicting the surface morphology of cpTi disks and Ti64 screws are shown in **Figure 1A**. Overall, both cpTi disk and Ti64 screw control specimens exhibited lustrous surfaces. Control cpTi disks presented scratches and marks characteristic of machining clearly visible, while the pristine implant Ti64 screw surface showed no signs of surface damage. After polarization treatment in 30% citric acid, both cpTi disks and Ti64 screws exhibited distinct changes in surface features, with a gold-purple discoloration characteristic of corrosion attack present across the entire specimen surface. For the cpTi disk specimens, surface marks due to machining were less pronounced, and the surface appeared to have become rougher. Moreover, the formation of what appeared to be pits was evident and indicative of pitting corrosion in the cpTi disks, and the surface roughness appeared to have qualitatively increased. Corrosion damage was especially prevalent along the Ti64 implant screw with cracks and apparent pitting formation present across the entire specimen surface.

Corrosion Behavior

Electrochemical testing was performed to evaluate the corrosion behavior of control and corroded cpTi disks and Ti64 screws. The values obtained for key electrochemical parameters, corrosion potential (E_{corr}), polarization resistance (Rp), corrosion rate (CR) and anodic Tafel slope (βa) of the control and corroded specimens are shown in **Figures 1B–E**. The E_{corr} values of the control cpTi disks and Ti64 screw specimens were higher than that of the cpTi and Ti64 corroded specimens. On the other hand, the Rp values of the cpTi corroded disks were higher than that of the control specimens while the opposite was observed for the Ti64 implant screw specimens. Corroborating the trends observed for Rp, the CR values of the control cpTi disk specimens were higher than that of the corroded cpTi

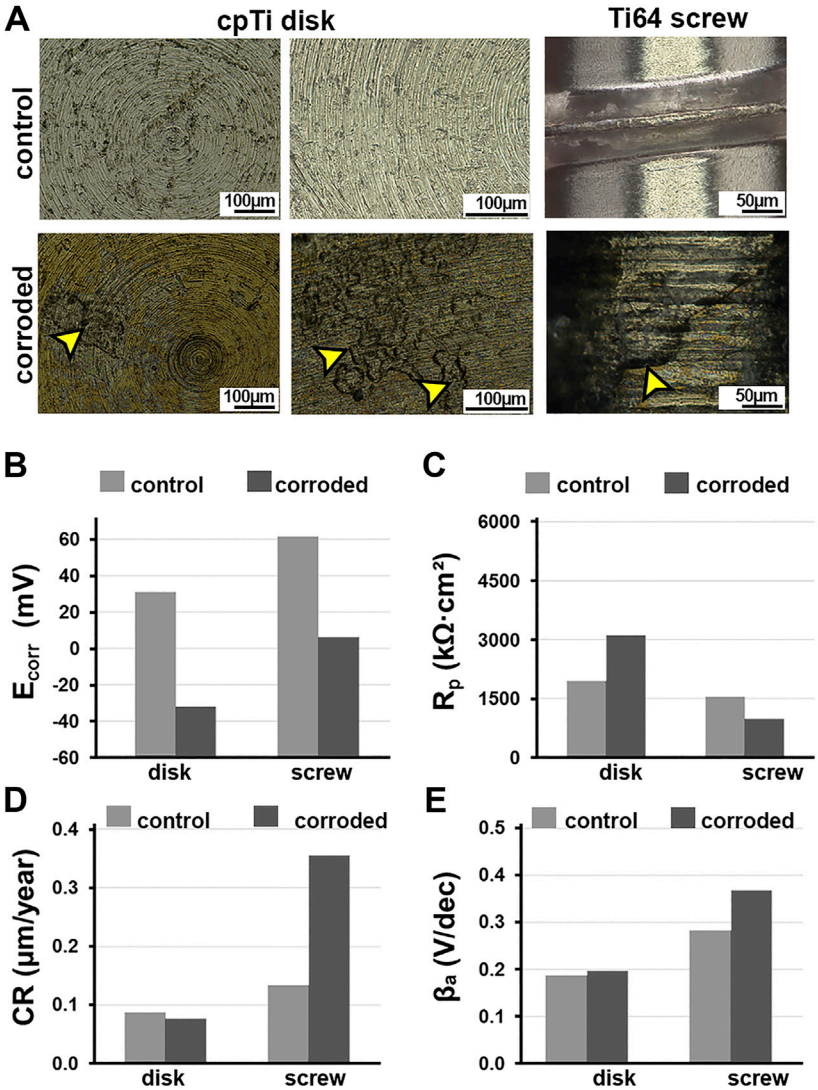

FIGURE 1 | (A) Representative surface morphology of cpTi disks and Ti64 screws treated by the electrochemical polarization in 30% citric acid. Signs of pitting damage are indicated by arrows. **(B)–(E)** One control or corroded (electrochemical polarization in 30% citric acid) disks or screws were evaluated for corrosion behavior: **(B)** Corrosion potential (E_{corr}), **(C)** polarization resistance (Rp), **(D)** corrosion rate (CR), and **(E)** anodic Tafel constant (βa) of control and corroded specimen.

specimens while the corroded Ti64 implant screw exhibited a corrosion rate about 2X greater in comparison to the control Ti64 screw. Despite being measured independently using separate electrochemical techniques, the general trend observed was that higher Rp values correlated with lower CR values. Finally, the βa values of corroded samples were marginally greater than that of the control specimens.

Surface Characterization by X-Ray Photoelectron Spectroscopy

XPS measurements were used to describe the chemical state of cpTi surface through shifts of binding energy of Ti2p3/2 peaks, which is well characterized. For elements like Ti, which exhibit doublet peaks due to a phenomenon known as spin orbit splitting, only the results associated with the Ti2p3/2 peaks are mentioned to avoid redundancy in the results section. The XPS results of the as cleaned, 1 min sputtered, and 2 min sputtered control and corroded (polarized in 30% citric acid) specimens are shown in **Figures 2A–D**. Surface analysis of the as cleaned cpTi disk specimens demonstrated the presence of native titanium oxide (TiO_2) that forms on Ti surfaces upon exposure to air or water across all specimen surfaces. Correspondingly, oxygen associated with TiO_2 and OH groups present on Ti surfaces were detected. The higher BE tail observed in the O1s spectra represents oxygen-containing species associated with adventitious carbon contamination, which decreased in intensity upon removal by sputtering. After sputtering the surface for 1 min, the lower Ti^{3+} and Ti^{2+} oxidation states present in sub-oxide layers were detected for both control specimens and specimens artificially corroded in 30% citric acid

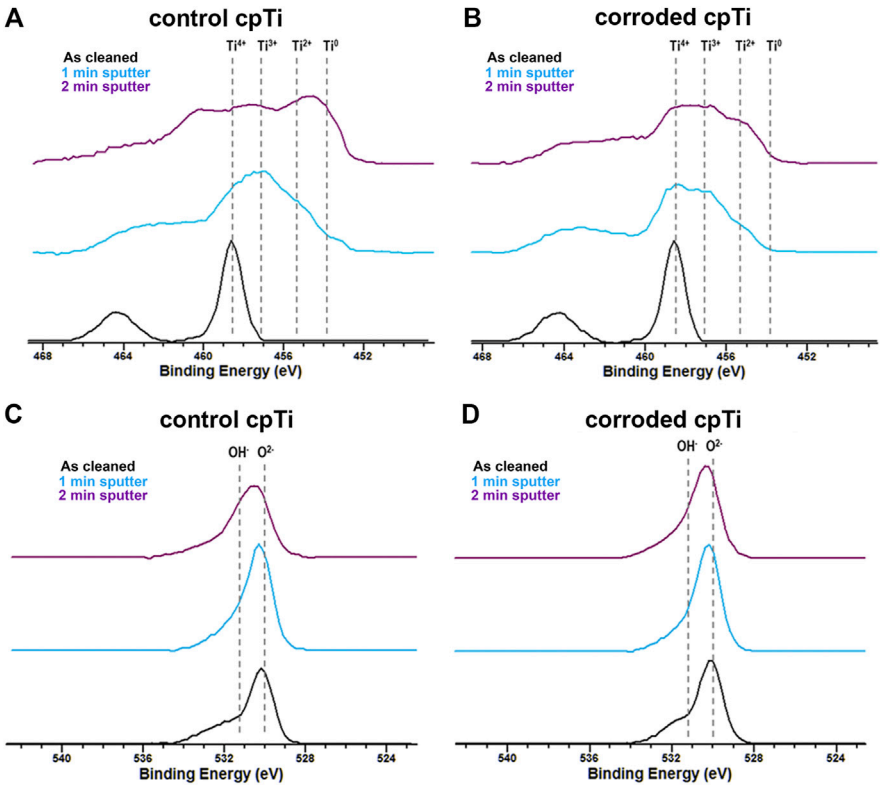

FIGURE 2 | Surface characterization of cpTi disks by X-ray Photoelectron Spectroscopy (XPS). **(A)** Ti2p spectra of **(A)** control and **(B)** corroded (electrochemical polarization in 30% citric acid) cpTi specimens as cleaned (black curves), after sputtering for 1 min (light blue curves), and after sputtering for 2 min (purple curves). O1s spectra of **(C)** control and **(D)** corroded cpTi specimens as cleaned (black curves), after sputtering for 1 min (light blue curves), and after sputtering for 2 min (purple curves).

in addition to Ti^{4+} oxidation state. After sputtering the surface for 1 more min (2 min in total), metallic Ti (Ti^{0}) was detected on the control specimen (**Figure 2A**) but not on the corroded ones (**Figure 2B**).

Histological Results of Subcutaneous Model Post-Control cpTi vs. Corroded cpTi Disks Implantation in Mice

Subcutaneous healing was evaluated at 3, 7, 14, and 21 days post control and corroded cpTi disk implantation using H&E description (**Figures 3A,B**) and histomorphometry (**Figure 3C**). Several parameters involved with healing and/or FBR were considered in this quantification, such as blood clot, inflammatory cells, FBGC, fibers, fibroblasts and blood vessels. As observed on H&E histological sections from the control cpTi group, a suitable blood clot formation and a slight mononuclear inflammatory infiltrate was noted at 3 days, followed by gradual connective tissue formation along 7–21 days, lacking FBGC while containing fibroblasts, fibers and negligible quantities of inflammatory cells surrounding regions of cpTi-disk implantation (**Figure 3C**). On the other hand, corroded cpTi specimens induced a strong FBR, with a significantly increased area density of mononuclear inflammatory cells at 3 days, presence of FBGC in all experimental periods, as well a significantly increased area density of blood vessels at 14 and 21 days, when compared to cpTi control. However, corroded cpTi implantation sites presented no statistical differences in area density of fibers and fibroblasts when compared to control cpTi group. Birefringence analysis revealed a gradual formation of yellow/red spectrum of collagen fibers surrounding control cpTi disks at 21 days. Decreased maturation of collagenous matrix was observed in the capsule surrounding the corroded cpTi group, especially considering reddish collagen fibers (**Supplementary Figures S1A,B**). Additionally, as demonstrated at higher magnification, FBGCs surrounding corroded cpTi disks spaces were found with phagocytic vacuoles containing foreign bodies (**Figure 3B**).

Immunolabeling for M1/M2 Macrophages Markers, and TRAP+ Cells on Sites of Control cpTi and Corroded cpTi Subcutaneous Implantation in Mice

Results from immunofluorescence of M1 and M2 macrophages by expression of CD80 and CD206 markers during 3, 7, 14, and 21 days post-implantation of control and corroded cpTi disks

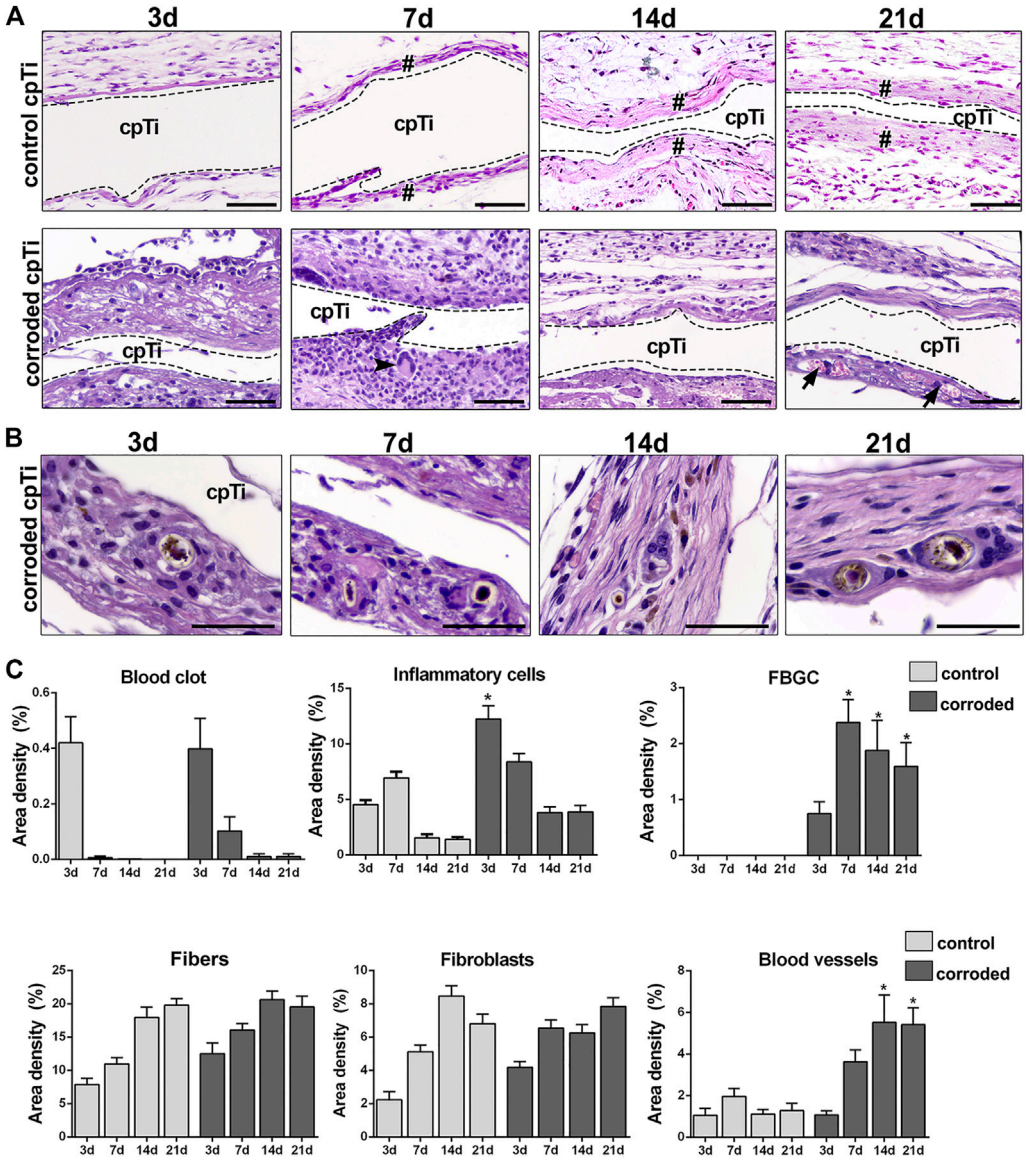

FIGURE 3 | Histopathological and histomorphometric characterization of C57Bl/6 mice subcutaneous tissue post implantation of control cpTi and corroded cpTi disks (electrochemical polarization in 30% citric acid). **(A), (B)** An intense inflammatory infiltration was found at 3 and 7 days near corroded cpTi disks implantation. From 7 days' time point, it was possible to detect collagen fibers deposition and resolution of inflammation in control cpTi disks implantation (#). FBGC (arrowhead) were found from 3 to 21 days surrounding the disks spaces (cpTi). At 14 and 21 days, both sites of cpTi disks implantation (control and corroded) presented a thick collagenous capsule formation. Corroded Ti disks presented an abundant amount of blood vessels at 14 and 21 days (arrows). H&E staining scale bars = 50 μm. **(C)** Quantification of parameters related to healing or FBR in subcutaneous sites of cpTi disks implantation from 3 to 21 days. Statistical tests: ANOVA followed by Bonferroni's multiple comparison post-hoc tests. *Indicates statistically significant differences in the same time point of the corroded vs. control group ($p < 0.05$).

demonstrated both groups with double-positive labeling for CD80 and CD206 markers (**Figure 4**). CD80 and CD206 were co-localized in mononuclear cells with characteristic morphology of macrophages (rounded nuclei and large cytoplasm) in areas surrounding the cpTi disks (spaces) in both groups (control and corroded) for 3 days. However, CD80+ cells were more predominant in corroded cpTi implantation sites, as observed at 21 days (**Figure 4**). TRAP+ cells (both macrophages and FBGCs morphologies) were found at corroded cpTi implantation sites but not at control cpTi sites (**Figures 5A,B**).

Gene Expression Patterns of Control cpTi vs. Corroded cpTi Disk Implantation in Subcutaneous Tissue of Mice

Samples from subcutaneous tissue subjected to control and corroded cpTi disk implantation were analyzed utilizing an exploratory RT-PCR array (**Figure 6**). Untouched subcutaneous tissue samples were used as control. Change between experimental groups (control or corroded cpTi) vs, control was considered significant when greater than 2-fold

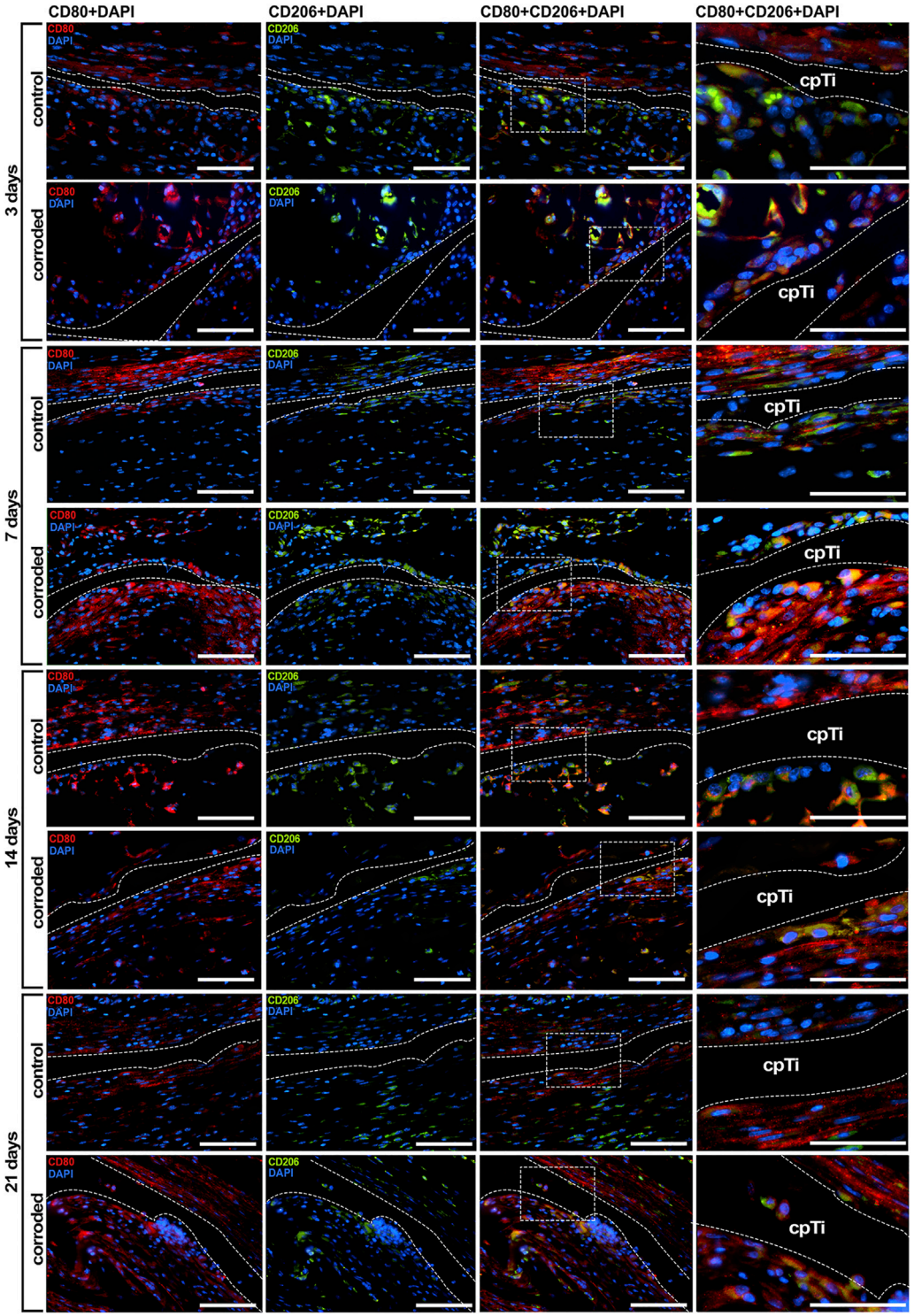

FIGURE 4 | Immunofluorescence analysis for M1 (CD80) and M2 (CD206) macrophages markers in subcutaneous implantation model in C57Bl/6 mice using control and corroded cpTi disks. Chronology of subcutaneous healing with M1 (CD80) and M2 (CD206) localization and co-localization is observed throughout 3, 7, 14, and 21 days. Fluorescence in blue = nuclei, red = CD80, green = CD206, yellow = CD80 + CD206. Scale bars = 50 μm. White dashed lines and cpTi indicate space previously occupied by cpTi disks.

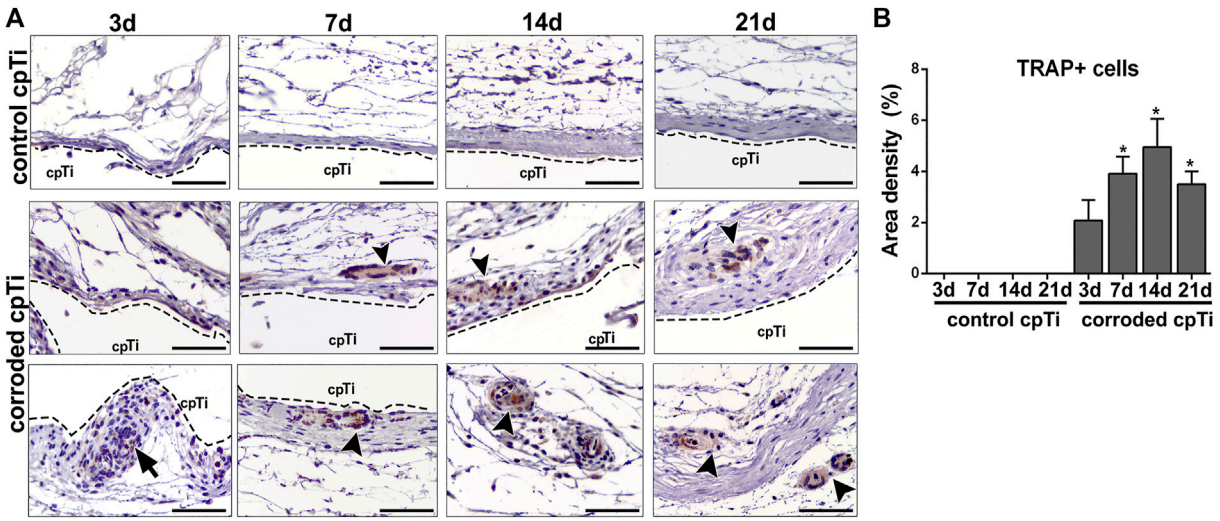

FIGURE 5 | Immunohistochemistry for TRAP+ cells surrounding the sites of control and corroded cpTi disk implantation in the subcutaneous tissue of C57Bl/6 mice throughout 3, 7, 14, and 21 days. **(A)** Representative images of subcutaneous tissue surrounding control and corroded cpTi disks. TRAP+ macrophages (arrow) and TRAP+ FBGC (arrow heads) are predominantly found at corroded Ti sites. Scale bars = 50 μm. **(B)** Quantification of TRAP+ cells from 3 to 21 days post-implantation of control and corroded Ti specimens by histomorphometric analysis. Statistical tests: ANOVA followed by Bonferroni's multiple comparison post-hoc tests. *Indicates statistically significant differences in the same time point of the corroded vs. control group ($p < 0.05$).

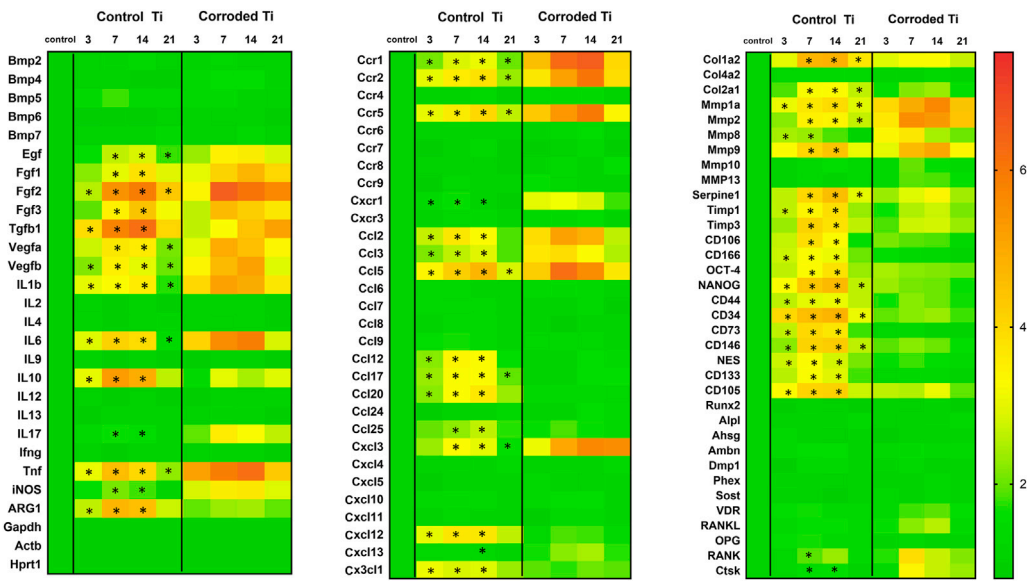

FIGURE 6 | Gene expression patterns of C57Bl/6 mice post implantation of control or corroded cpTi disks in subcutaneous tissue. Untouched subcutaneous samples were used as tissue control for gene expression normalization. Molecular analysis of the gene expression patterns in the region of cpTi disks implantation was performed by real-time PCR array for each experimental group (control, control cpTi and corroded cpTi), considering 5 independent samples for each experimental period (3, 7, 14, 21 days) and two technical replicates. Results are depicted as a heat map representing the mean fold increase change in mRNA expression from the 5 independent samples measurements to the control samples and normalized by internal housekeeping genes (Gapdh, Hprt, Actb). *Indicates statistical significance in gene expression between at control cpTi and corroded cpTi groups, data analysis was performed by using RT2 Profiler software.

up, as represented in the heat map (**Figure 6**). In general, when comparing the subcutaneous samples from control cpTi vs. corroded cpTi implantation, it was observed that corrosion significantly altered the dynamics of expression of several growth factors (Egf, Fgf1, Fgf2, Fgf3, Tgfb1, Vegfa, Vegfb), pro-inflammatory markers (IL1b, IL6, IL17, Tnf, iNOS),

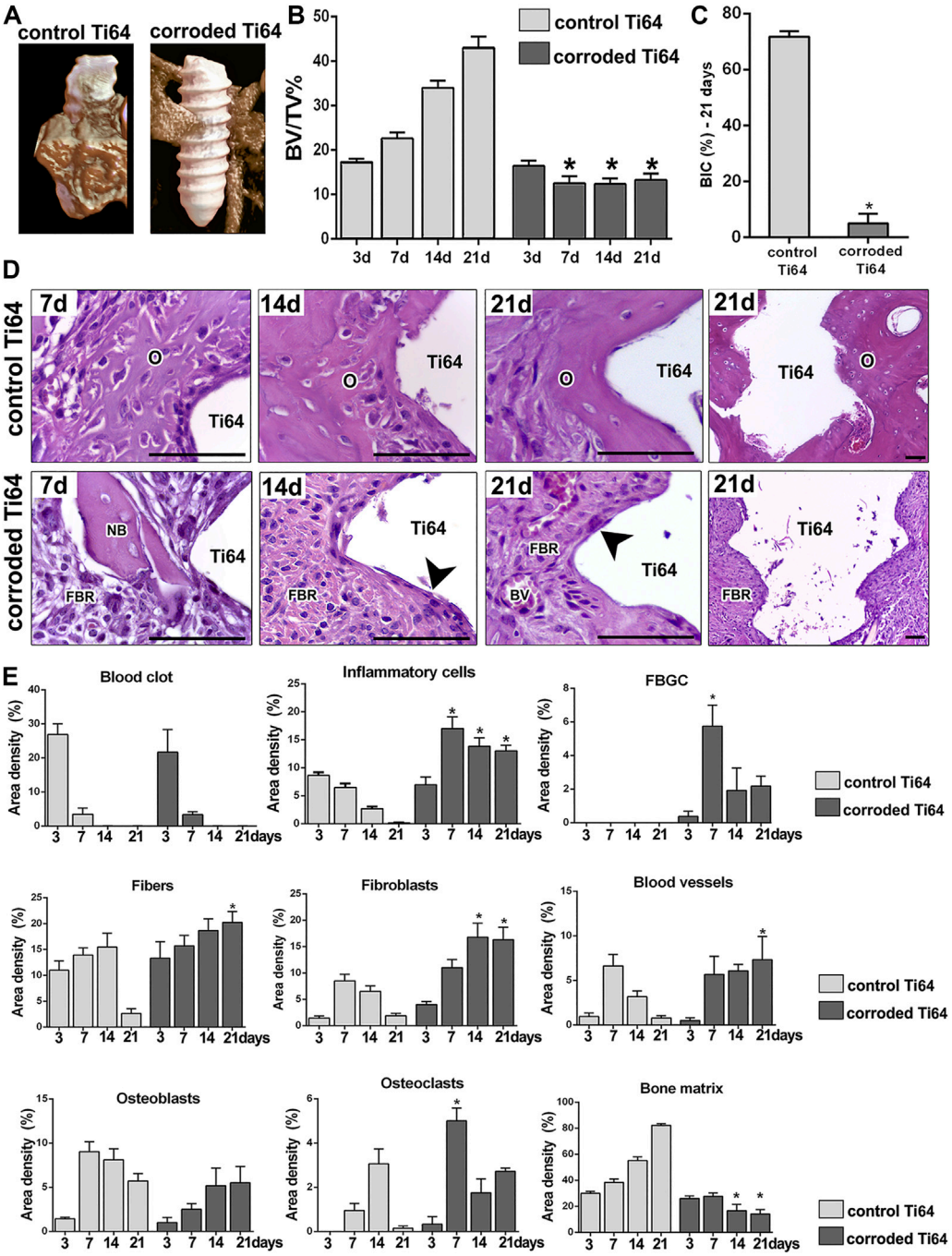

FIGURE 7 | Microscopic analysis for osseointegration outcomes in the edentulous ridge of maxilla following control and corroded Ti64 screw implantation in C57Bl/6 mice. **(A)** MicroCT showing three-dimensional representative images obtained with the CT-Vox software at 21 days post-screw implantation and **(B)** bone volume/tissue volume (BV/TV, %) in the interface bone-screw after 3, 7, 14, and 21 days post-implantation for control and corroded Ti64; ANOVA followed by Bonferroni's multiple comparison post-hoc tests was used for statistical analysis. **(C)** BIC % was obtained at 21 days using ImageJ software (Version 1.51, National Institutes of Health); Mann–Whitney test was used for statistical analysis. **(D)** Histopathological analysis for chronology of oral osseointegration is observed throughout 7, 14, and 21 days in control and corroded Ti screws implantation sites. Histological slides were stained with H&E and images are shown at ×100 magnification (7, 14 and ×21 d), and ×10 magnification for 21 days. Ti, Ti screw space; Arrowheads–FBGC; O, osseointegration; NB, Necrotic bone; FBR, Foreign Body Reaction. Scale bars = 50 μm. E) Histomorphometric analysis of healing or FBR components at the Ti-bone interface after 3, 7, 14, and 21 days post-implantation for control and corroded groups. In E, Kruskal–Wallis test followed by Dunn's was used for blood clot, FBGC, Osteoclasts and Blood vessels. The remaining parameters were analyzed by ANOVA followed by Bonferroni's multiple comparison post-hoc tests. In B, C and E, quantitative analysis are presented as the mean and SD from six biological replicates from each group and time point. *Indicates significant statistical differences ($p < 0.05$) in comparison with control.

anti-inflammatory markers (IL10, ARG2), different families of chemokines and chemokine receptors (Ccr1, Ccr2, Ccr5, Cxcr1, Ccl2, Ccl3, Ccl5, Ccl12, Ccl17, Ccl20, Ccl25, Cxcl3, Cxcl12, Cxcl13, Cxc3cl1), matrix markers (Col1a2, Col2a1, Serpine1, Mmp1a, Mmp2, Mmp8, Mmp9, Timp1, Timp3), putative markers for stem cells (CD106, CD166, OCT-4, NANOG, CD44, CD73, CD146, NES, CD133, CD105), as well markers related with FBGC activity (RANK and Ctsk). In comparison with control cpTi, corrosion products induced higher gene expression for Fgf2, Vegfb, IL6, Tnf, chemokines and receptors involved with leukocyte infiltration (Ccr1, Ccr2, Ccr5, Cxcr1, Ccl2, Ccl3, Ccl5), matrix metalloproteinase markers (mmps1a and 8), from 3 to 14 or 21 days, as demonstrated in the heat map (**Figure 6**). Other growth factors (Egf, Fgf1, Fgf3, Vegfa), inflammation markers (IL17, iNOS, Cxcl3) and matrix degradation markers related to metallopeptidases (Mmps) genes (Mmp2 and 9) were upregulated in corroded cpTi group vs. control cpTi from 7 days and continued with higher expression until 14 days (Fgf1, Fgf3, IL17, iNOS, Mmp9) or 21 days (Egf, Vegfa, Mmp2, Cxcl3). On the other hand, a decreased expression of M2 markers (Tgfb1, IL10, ARG2) was observed in corroded cpTi vs. control cpTi from 3 to 14 days. In addition, corroded samples presented a decrease in the expression of several chemokines (Ccl12, Ccl17, Ccl20, Ccl25, Cxcl12, Cx3cl1) and several stem cell markers from 3 days to 14 or 21 days. Markers related to matrix formation and maturation (Col1a2, Col2a1, Serpine1, Timp1, Timp3) were significantly upregulated in control cpTi vs. corroded cpTi during the course of subcutaneous tissue healing. Finally, additional targets specific for bone were included in the panel of subcutaneous tissue but were used as additional control for the next molecular analysis.

Microscopic (MicroCT and Histology) Results of Corrosion Effects on Oral Ti64 Osseointegration Model in Mice

Regarding the effects of corrosion of Ti-based devices on osseointegration, oral Ti64 screw implantation in mouse was conducted (**Figure 7**). The microCT and histological results, including BIC, clearly demonstrated failure on corroded implants following oral implantation in C57Bl/6 mice (**Figures 7A–E**). MicroCT revealed a significantly lower quantity of BV/TV% surrounding corroded Ti64 surfaces throughout 7–21 days as compared to control Ti64 surfaces at the same evaluation points (**Figures 7B**). Following BIC evaluation (**Figure 7C**), control Ti64 screws presented 71.77 ± 5.72 BIC% at 21 days, while osseointegration failures in corroded Ti64 screws presented 5.02 ± 9.69 BIC%. Microscopically, osseointegration failure is accompanied by a strong FBR toward corroded Ti64 threads, with arrangement of FBGCs surrounding the implant bed. A significantly higher area density of inflammatory cells, fibroblasts and blood vessels is observed at sites under Ti64 corrosion at the later stages of implantation when compared to control Ti64 screws (**Figure 7E**). In addition to the lack of bone formation surrounding the corroded Ti64 screws, strong bone resorption is noted on this group, with higher area density of osteoclasts at 7 days as compared to control Ti64 group. Additionally, there was a decreased quantity of BV/TV (%) and bone matrix area density at corroded Ti64 compared to control Ti64 at the early stage (7 days) post-implantation (**Figures 7B,E**). The histomorphometric analysis revealed higher density of inflammatory cells throughout 7, 14 and 21 days at corroded Ti64 as compared to controls, accompanied by the significant area density of FBGC and osteoclasts at 7 days, as well an increased area density of fibroblasts and decrease in bone matrix at 14 and 21 days (**Figure 7E**).

Gene Expression Patterns of Control Ti64 vs. Corroded Ti64 Screw Implantation in Oral Osseointegration Model in Mice

Samples from all periods post-implantation of Ti64 screws was analyzed by an exploratory RT-PCR array (**Figure 8**), considering the same molecules analyzed in the subcutaneous samples and additional targets specific for bone. Gene expression for control and corroded Ti64 screws was depicted as the fold increase change related to tissue control samples, which were from the right side of maxilla of C57Bl/6 mice (no surgery). Corrosion in Ti64 screws induced a higher expression of fibroblast growth factors (Fgf1 and Fgf2) from 3 to 14 days as compared to the control Ti64 group. In general, pro-inflammatory markers, such as IL1b, IL6, Tnf and IL17 were also significantly upregulated in corroded Ti64 group from 3 to 7 (IL17), 14 (IL1b) or 21 days (IL6 and Tnf) in corroded Ti64 group vs. control Ti64. A M1 marker (iNOs) was upregulated in corroded Ti64 group vs. control at 7 and 14 days. M2 macrophage markers Tgfb1 and IL10 presented an increase in control Ti64 group vs. corroded Ti64 group from 3 to 14 days (IL10) and 21 days (Tgfb1), while ARG1 was significantly upregulate at 7 and 14 days post screw implantation. Several chemokine and chemokine receptors were differently upregulated in corrosion group vs. control during the time points following the osseointegration. Ccr1, Ccr2, Ccr5, Cxcr1, Ccl2, Ccl5, Ccl3, Cxcl3 were upregulated from initial periods post screw implantation (3 or 7 days) under corrosion condition when compared to control screws. On the other hand, mRNA levels of Cc112, Ccl17, Ccl20, Ccl25 and Cx3cl1 were increased in control Ti64 group vs. corroded Ti64 group lasting until the later periods. Among the genes for extracellular matrix markers, Col1a2 was upregulated in control Ti64 vs. control tissues from 7 to 21 days, while Mmp1a, Mmp2 and Mmp9 were upregulated in corroded Ti64 vs. control Ti64 in these same time points. Considering stem cells putative markers, mRNA levels of CD106, CD166, OCT-4, NANOG, CD34, CD73, CD146, CD105, and Cxcl12 were significantly increased in control Ti64 samples vs. corroded Ti64 from 3 days and until the maturation phase (14 and 21 days). Finally, bone differentiation markers Bmp2, Bmp4, Bmp7, Runx2 and Alpl presented increased expression in

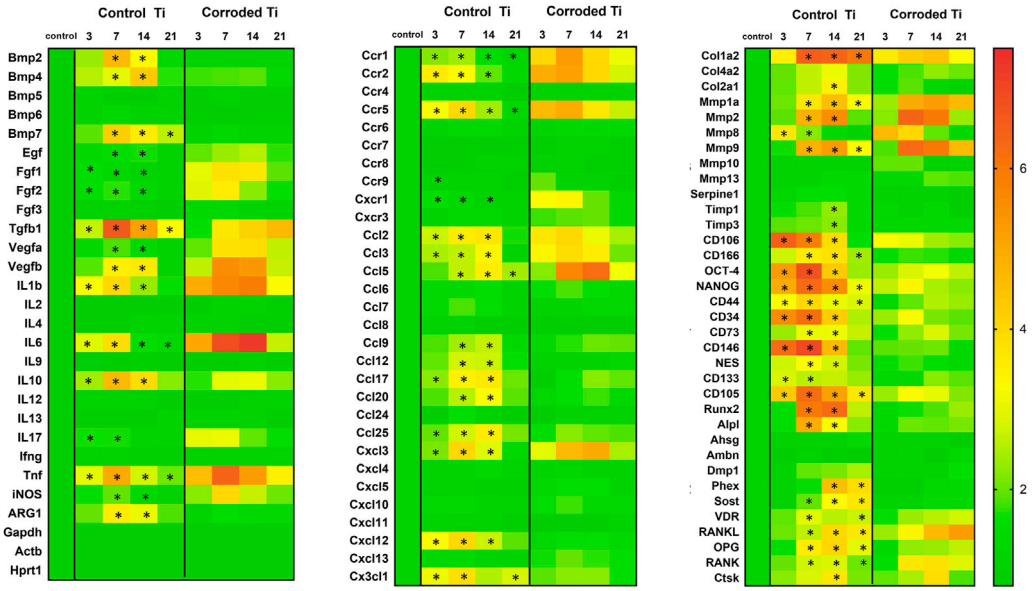

FIGURE 8 | Gene expression patterns from C57Bl/6 mice maxillary bone samples subjected to control or corroded Ti64 screw implantation. Untouched bone maxillary bone samples were used as tissue control. Molecular analysis of the gene expression patterns in the region of Ti64 screw implantation was performed by real-time PCR array for each experimental group (control tissue, control Ti64 and corroded Ti64), considering 4 independent samples for each experimental period (3, 7, 14, 21 days) and two technical replicates. Results are depicted as a heat map representing the mean fold increase change in mRNA expression from the 4 independent samples measurements to the control samples and normalized by internal housekeeping genes (Gapdh, Hprt, Actb). *Indicates statistical significance in gene expression between at control cpTi and corroded cpTi groups, data analysis was performed by using RT2 Profiler software.

control Ti64 vs. corroded Ti64 from 7 days, in addition to osteocyte markers Dmp1, Phex, Sost and VDR which appeared upregulated from 7 or 14 days during the osseointegration. On the other hand, RANKL and RANK mRNA levels were increased at corroded Ti64 sites vs. control Ti64 sites from 7 to 21 days, while OPG mRNA levels were increased in control Ti64 samples vs. corroded Ti64 samples in the same periods. Detailed gene expression analysis is represented in **Figure 8**.

DISCUSSION

Corrosion of metallic based devices is a well reported challenge in the field with a number of studies discussing its impact on implant performance and host tissues (Cadosch et al., 2009; Mombelli et al., 2018; Noronha Oliveira et al., 2018; Hanawa, 2019; Dini et al., 2020). Corrosion of Ti-based devices can induce exacerbated and chronic host inflammatory response, resulting in unfavorable osseointegration outcomes (Mouhyi et al., 2012; Noronha Oliveira et al., 2018). Therefore, the host response to Ti and its alloys seems to play a crucial role in osseointegration predictability. Specifically, understanding biological mechanisms triggered in response to corroded metals may contribute to the improvement of biomaterials and/or prevention of osseointegration failures. In the present study, we used an electrochemical protocol in 30% citric acid (pH ≈ 2) to produce electrochemical attack on the material surface and to induce accelerated corrosion on Ti-based devices (cpTi or Ti64) surface and in order to recapitulate corrosion features observed in retrieved implants (Rodrigues et al., 2013; Arteaga et al., 2021). Then, we comprehensively characterized the cellular and molecular host response toward the corroded cpTi surfaces in the subcutaneous tissue of C57Bl/6 mice. Finally, we characterized the detrimental effects of Ti64 corrosion products on bone, providing a histological and molecular characterization of early failure related to corrosion in comparison to successful oral osseointegration of Ti-based devices.

Different methods (UV, electrochemical, biological aging) have been used to induce corrosion on the surface of Ti/Ti alloys with the goal of inducing damage on Ti surface as it can occur in the challenging conditions *in vivo*, such as due to pH variation, infection and/or inflammation (Messer et al., 2009; Messer et al., 2010; Chandar et al., 2017). It is important to consider that methods used to accelerate Ti corrosion *in vitro* are not designed to reproduce an inflammatory or infectious environment but are useful to reproduce the surface changes comparable to those observed in Ti devices retrieved from *in vivo* conditions. In our study, cpTi disks and Ti64 screws were treated with electrochemical polarization in 30% citric acid at 9 V for 20 min (**Figure 1**). Our results demonstrated that electrochemical polarization of cpTi disks and Ti64 screws in 30% citric acid solution resulted in the surface coloration (yellow and purple) as compared to the controls (**Figure 1**).

Our findings also demonstrated the method used to induce corrosion damage on both specimens (disks and screws) resulted in detrimental effects on morphological features of tested samples (etching of machining marks, apparent local pit formation, and increased surface roughness) comparable to other *in vitro* studies (Sridhar et al., 2016), corroded cpTi dental implants (Rodrigues et al., 2013; Sridhar et al., 2018) or cpTi and Ti alloy based abutments retrieved from patients (Wheelis et al., 2018; Jain et al., 2020).

Next, electrochemical testing of control and corroded Ti samples provided a means for evaluating corrosion behavior. In general, higher E_{corr} values indicate a greater degree of thermodynamic stability, which in general is positively correlated with the duration of exposure to aqueous media. That is, the passive oxide layer on the cpTi disk and implant screw control specimens was more stable than that of the corroded specimens. However, polarization resistance (Rp) directly quantifies a material's corrosion resistance. In this regard, cpTi disks treated with electrochemical polarization exhibited the greatest degree of corrosion resistance compared to the controls. This behavior was expected as electrochemical polarization accelerates surface oxidation. However, depending on the geometry of the device and magnitude of the applied potential, the oxide layer could become too thick and susceptible to rupture due to buildup of internal stresses. This may explain why the corroded disk specimens with exposed flat surfaces had higher Rp values than the control while the corroded implant screw actually had a lower Rp value. That is, the greater degree of sharp edges and corners on the threads of the implant screw could have generated cracks which are prone to localized corrosion. As a material's corrosion resistance (Rp) increases, its corrosion rate (CR), or rate of metal ion dissolution, decreases proportionally according to the Stern-Geary equation. Corroborating this trend, corrosion rates were observed to be higher for the control cpTi disk vs. its corroded counterpart while the corroded Ti64 screw had a higher CR value than the control Ti64 screw. This corrosion behavior for the cpTi disks and Ti64 screws was further validated as Rp and CR were measured independent of one another (Rp: linear polarization resistance; CR: anodic Tafel polarization). Thus, treatment with electrochemical polarization in 30% citric acid passivated the surface and led to lower CR and higher Rp values for the Ti disk but not Ti screw. A previous corrosion study of failed Ti-based devices retrievals also had higher average E_{corr} and Rp and lower CR values than control (Sridhar et al., 2018). Finally, the anodic Tafel slope (βa), which is sensitive to the electrochemical environment and surface conditions, was higher for electrochemical attack vs. control, suggesting that the treatment modified the electrochemical behavior of Ti (**Figures 1–E**).

In our study, both cpTi control and treated disks had an intact oxide layer based on XPS analysis. Overall, carbon (C), titanium (Ti) and oxygen (O) were primarily detected on all samples along with minute quantities of calcium (Ca), silicon (Si), nitrogen (N) and lead (Pb). Contamination of the oxide layer is expected due to trace amounts of the latter elements in air and aqueous environments. To remove superficial surface layers and assess the relative oxide layer thickness, control and corroded surfaces were sputtered for 2 min prior to XPS scans (**Figures 2A–D**). For the control, Ti in its native oxide state (TiO_2) in addition to subsurface oxides (Ti_2O_3 and TiO) were detected (**Figure 2A**), which is in accordance with a previous study (Gindri et al., 2015). Accordingly, oxygen was found to be bonded to Ti (TiO_2) and as hydroxyl groups (OH) (**Figure 2B**), which agrees with previous studies (Gindri et al., 2015). Further comparisons between the Ti and O spectra of control vs. treatment with electrochemical polarization as cleaned and after 1 or 2 min of sputtering are shown in **Figures 2A–D**. The lower intensity (amount) of Ti on the as cleaned surface after electrochemical polarization vs. control was due to citric acid adsorption on TiO_2 (Souza et al., 2015), yielding a thicker passivation layer. Thus, longer sputtering times were needed to expose subsurface oxides (Ti_2O_3 and TiO) after electrochemical polarization relative to control. This behavior is in agreement with observations for Ti healing abutments after placement in the oral cavity (Olmedo et al., 2012). Overall, these findings suggested that only electrochemical polarization treatment yielded a surface distinct from control and possessed corrosion behavior and oxide layer composition similar to Ti devices after exposure to the oral environment. In spite of the relatively high corrosion resistance of Ti, it is still susceptible to corrosion under biological environmental conditions, as previously demonstrated in failed retrievals (Rodrigues et al., 2009; Rodrigues et al., 2013; Gindri et al., 2015). Although the number of replicates for electrochemical tests in this study was reduced, electrochemical polarization was considered as a valid method to induce damage on Ti-based specimens surface mimicking damage observed in implants that underwent corrosion process *in vivo*, which resulted in unfavorable clinical outcomes.

Next, control and corroded cpTi disks were implanted in the subcutaneous tissue of mice. Interestingly, the reaction of soft tissue surrounding metallic implants has been previously evaluated comparing Ti-based biomaterials with different type of materials (Suska et al., 2003) or coatings (Wheelis et al., 2020) in rats, modified Ti alloys (silver thiolate-modified Ti) (Tîlmaciu et al., 2015), and pharmacologic treatments following cpTi-disk implantation in mice (Biguetti et al., 2019). When Ti is compared with copper, the resulting connective tissue capsule around copper displayed a higher amount of macrophages and FBGC and higher levels of pro-inflammatory cytokines (Suska et al., 2003). In previous studies, cpTi disk implantation in subcutaneous tissue was followed by a mild and transitory inflammatory response (Biguetti et al., 2019; Wheelis et al., 2020), and a well-tolerated response has also been shown with modified Ti alloys (silver thiolate-modified Ti) (Tîlmaciu et al., 2015). Accordingly, our results from control cpTi groups implanted in subcutaneous tissue demonstrated a constructive and mild inflammation along with gradual

deposition and remodeling of the collagenous matrix in subcutaneous tissue, with no evidence of FBGC formation (**Figure 3**).

Biocompatibility *in vivo* is observed when the biomaterial is able to trigger and support an appropriate healing process and does not elicit a damaging immune response in the host tissues (Hanawa, 2019). Importantly, adequate biomaterials-associated tissue healing has been also related to the balance of macrophages polarization into functional M1 and M2 phenotypes, in which Ti-based biomaterial surface is preferentially surrounded by M2 macrophage phenotypes (Sridharan et al., 2015). In addition, the successful subcutaneous healing process to cpTi control was linked to the upregulation of M2 (Tgfb1, IL10 and ARG1) and stem cell markers from 3 to 14 days post implantation, as expected by the regenerative role of M2 macrophage subset (Biguetti et al., 2019; Pajarinen et al., 2013; Sridharan et al., 2015; Hallab and Jacobs, 2017)c(**Figure 6**). It is clear that the corrosion damage disrupted cpTi disk biocompatibility and induced a strong FBR in the subcutaneous tissue of mice, featured by a persistent inflammatory process from initial time point (3 days) and lasting until later time points 14 or 21 days. This dysregulated response resulted in a disorganized fibrous tissue containing higher amount of blood vessels and inflammatory cells throughout 21 days (**Figure 3**). It has been shown that debris released from metallic biomaterials, including Ti, can induce predominant activation macrophages with the persistent release of inflammatory cytokines, chemokines and chemokine receptors (Pajarinen et al., 2013; Hallab and Jacobs, 2017). Indeed, human macrophages, undifferentiated (M0) or differentiated to M1 and M2 phenotypes, develop a specific response to Ti particles. M1 macrophages respond to Ti particles with increased production of pro-inflammatory cytokines (IL6, TNFα, IL1β) and chemokines (CXCL1, CCL22, CCL11, CCL3, and growth factors (FGF2, EGF, VEGF) (Pajarinen et al., 2013). In addition, M2 differentiated macrophages exposed to Ti particles suppress production of IL-10 and promote production of IL-8, CCL7 and IL-1a. In response to Ti particles, M1 presented a decreased phagocytic activity while M0 and M2 macrophages were able to engulf released materials (Pajarinen et al., 2013). Indeed M2 macrophages present higher expression of CD206 (mannose receptor), which mediates phagocytosis (Wainszelbaum et al., 2006) and has been suggested to mediate particle uptake (Pajarinen et al., 2013). In agreement with all these findings, the predominance of enhanced M1 type response to corroded cpTi surfaces was supported by increased mRNA levels of pro-inflammatory cytokines (IL1b, IL6, and TNF) and iNOS (**Figure 6**). Unremitting inflammation was also associated with higher expression of several chemokine receptors and related chemokines involved in monocyte/macrophage infiltration (e.g., Ccr1, Ccr2, Ccr5, Ccl2, Ccl3, Ccl5) (**Figure 6**), consequently sustaining a detrimental inflammatory loop at cpTi corroded sites. Also, a mix of M1 (CD80+ mononuclear cells) and M2 (CD206+ mononuclear cells) phenotypes were found in both subcutaneous sites of control and corroded cpTi disks implantation by immunofluorescence (**Figure 4**). The increased release of cytokines and chemokines has also been previously demonstrated to disturb phagocytosis by macrophages in other studies, resulting in their fusion to form FBGC on a biomaterial (Hallab and Jacobs, 2017; Mariani et al., 2019). As a signature of biomaterial-induced FBR, the presence of FBGC was marked at all periods post corroded cpTi samples in H&E (**Figure 3**), with phagocytic vacuoles containing foreign bodies mainly found in FBGC cytoplasm and TRAP positive staining (**Figures 5A,B**). These findings were consistent with other studies in rats where cpTi corrosion led to release of corrosion products at the host-biomaterial interface, specifically near blood vessels and internalized by macrophages (Olmedo et al., 2008).

The subcutaneous model provided useful insights into how connective tissue/mesenchymal components may react to the biomaterial with and without corrosion alterations. Additionally, the model provided a sufficient amount of samples to evaluate host response by different histological (histopathology, immunohistochemistry, and immunofluorescence) and molecular (RT-PCR) approaches, especially comparing subcutaneous sites with the limited dimensions of bone implantation sites available in mice (Biguetti et al., 2019). Of note, bone is precisely a specialized connective tissue, with peculiar features regarding the mineralized matrix. During the osseointegration process, an intramembranous process with deposition of connective tissue is temporally required, under the control of a well-orchestrated inflammatory response (Biguetti et al., 2018; Wheelis et al., 2021). In the context of this early inflammation and considering the nature of both connective tissues, the subcutaneous model is viable to understand the general features of the inflammatory response and/or FBR to the corroded biomaterial. However, titanium implantation follows a well-orchestrated inflammatory response that ultimately leads to bone apposition in osseointegration model (Davies, 2003; Biguetti et al., 2018; Wheelis et al., 2021), while in connective tissue, it leads to a well-organized capsule with no evidence of FBGC (Biguetti et al., 2019; Wheelis et al., 2020). Thus, the gradual differentiation of bone cells and bone deposition is another sophisticated step that required additional investigation in this study.

The effects of corrosion products from Ti alloy devices on osseointegration were evaluated using Ti64 screws implanted in C57Bl/6 mice maxillae. Control Ti64 group achieved osseointegration, and the events underlying the successful bone formation toward the biomaterial were in agreement with our previous findings using this model with Ti64 screw implantation in mice (**Figure 7**) (Biguetti et al., 2019; Biguetti et al., 2018; Mouraret et al., 2014) and also supported by other similar models using cpTi screws in rats (Wheelis et al., 2021; Lin et al., 2011). Concurrently with the histological findings, a mild and transient inflammatory response was followed by new bone deposition and remodeling (**Figure 7**), and the Ti64 control induced a M2-type response with increased stem cell and bone expression markers (**Figure 8**). Conversely, the corrosion of Ti64 screw completely altered the expression of M2 and MSC markers associated with a strong failure response at the bone-biomaterial interface. These results agreed with the subcutaneous model findings using cpTi disks and other

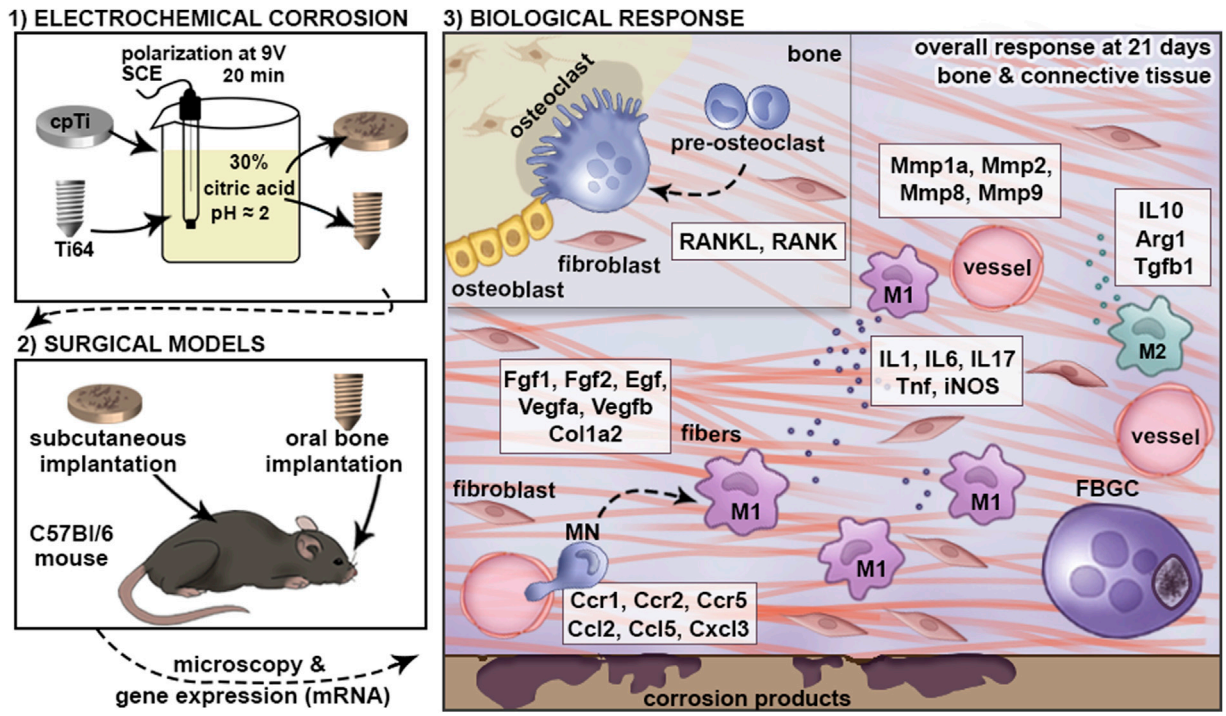

FIGURE 9 | 1) Protocol performed to induce accelerated corrosion on cpTi disks and Ti64 screws. 2) Surgical models on the subcutaneous and maxillary bone of C57Bl/6 mouse were used to evaluate the biological response to corrosion products. 3) Overall biological response at 21 days post corroded disk or screw implantation in connective tissue and bone, respectively.

microscopic studies using cpTi implants placed in rat tibias (Olmedo et al., 2008). FBGCs were found surrounding the implant bed and Ti64 threads, along with chronic mononuclear inflammatory infiltrate, fibroblasts and blood vessels throughout the 21 days post-implantation (**Figure 7C**). Despite leukocytes being the primary cells involved in Ti-device implantation response, MSCs may also be a target for Ti debris. Ti debris can reduce MSC viability, proliferation and osteogenic differentiation and induce the production of IL-1b and TNFα (Haleem-Smith et al., 2012).

Osteolytic activity at bone sites was evidenced by decreased amount of bone volume (**Figures 7B,C**) and a higher quantity of osteoclasts at 7 and 21 days (**Figure 7C**). In agreement with the microscopic results, the exploratory RT-PCR array revealed upregulated markers for fibrosis, chronic inflammation, and M1-type response in Ti64 corroded samples (**Figure 8**). In agreement, we detected an increased expression of chemokines and chemokine receptors involved in leukocytes recruitment, such as monocytes/macrophages (Ccr1, Ccr2, Ccr5, Ccl2, Ccl5) and increased expression of TNFα, IL6 and ILβ. Additionally, markers indicating peri-implant tissue destruction (RANK, RANKL, Mmp1α, Mmp2 and Mmp9) were significantly increased in Ti64 corroded samples compared to control Ti (**Figure 8**). It is known that the persistent secretion of pro-inflammatory cytokines such as IL-1b and TNFα is associated with bone resorption surrounding dental implants (Trombone et al., 2016; Gomes et al., 2019), as well as the increased transcription of MMP genes (Trombone et al., 2016). Additionally, patients with orthopedic implant aseptic loosening present elevated levels of IL-1b, IL-8, and TNFα in their synovial fluid, which is also associated with tissue destruction (Hernigou et al., 1999). Interestingly, in a model of oral osseointegration in rats, the release of Ti ions can be detected in gingival and bone tissues surrounding the implantation sites, and it can be associated with increased the expression of Ccl2 and the ratio of RANKL/OPG in gingival tissues (Wachi et al., 2015). These studies suggest that Ti ions may be partly responsible for the infiltration of monocytes and osteoclast differentiation at infection and osteolysis sites. In this same previous study, the authors loaded the gingival tissue with Ti ions (9 ppm) and exposed to *Porphyromonas gingivalis* LPS, demonstrating a synergistic effect of corrosion and infection on the inflammation and bone resorption around Ti implants (Wachi et al., 2015). Of note, in our study, the subcutaneous analysis was performed under aseptic conditions, and the osseointegration model did not involve the inoculation of pathogens associated with peri-implantitis, therefore limiting variables related to the host response to microorganisms and their products. Indeed, we used an aseptic surgical technique for implant placement in the oral cavity, and implant heads were only exposed to the mice commensal microbiota, which does not seem to negatively affect the screw surface, since Ti64 controls presented successful osseointegration.

Branemark defined osseointegration as "a direct contact between a loaded implant surface and bone at the light microscopical level of resolution", a concept which was published years later after the first use of the "osseointegration" term in the literature (Albrektsson et al., 1981). As recently reviewed, several alternative theories have been added to the concept of osseointegration, based on Ti/host biomechanical interactions and functionality (more applied to clinical studies, chemical bond between Ti and bone, and as foreign body response driven by bone) (Albrektsson et al., 2017). Chemical interactions based on osseointegration relies on the hypothesis in which the Ti/host interface represents a combination of local favorable chemical connections between the oxide layer and bone, but it is also assumed that Ti has a bioinert behavior (Albrektsson et al., 1981; Donath et al., 1992). While the chemical composition is demonstrated to cooperate with Ti surface properties, our results point to an additional immunomodulatory behavior beyond the inert property Ti surfaces have been indicated to possess (Albrektsson et al., 1981; Albrektsson et al., 1983). Considering the concept of osseointegration as a favorable FBR, it suggests that bone development around Ti-based implants might be a favorable protective bone response to isolate Ti from other tissues (Donath et al., 1992). Based on this theory, since bone belongs to connective tissues, the newly formed bone surrounding Ti implants may be considered as a calcified connective tissue reaction encapsulating the biomaterial. In our present study, we demonstrated that Ti-mediated osseointegration is driven by a well-orchestrated immune response toward bone differentiation, without key features of classic FBR, such as the presence of FBGC and fibrosis. FBR surrounding corroded samples was characterized by a strong and persistent chronic inflammation in connective tissue and bone and linked to the upregulation of fibrosis and pro-inflammatory markers.

In this study, corrosion damage of cpTi and Ti64 induced exacerbated inflammatory response in both connective tissue and bone, respectively. Considering particularly the oral osseointegration model, it is important to emphasize that Ti64 also contain other metals, such as V and Al, which are also cytotoxic along with Ti particles (Noronha Oliveira et al., 2018). Despite the study limitations in working with two different biomaterials and in distinct sites of the *in vivo* implantation, a similar pattern of inflammatory dysregulation linked to the upregulation of fibrosis and pro-inflammatory environment resulting in unfavorable healing outcomes was observed using both corroded cpTi and Ti64 devices. Therefore, this study confirmed that electrochemical corrosion of cpTi and Ti64 adversely altered the immunomodulatory properties of Ti-based biomaterials. Specifically, corrosion of Ti-based biomaterials induced exacerbated inflammatory response in both connective tissue and bone, linked to the upregulation of fibrosis, pro-inflammatory and osteoclastic markers and resulting in unfavorable healing and osseointegration outcomes (**Figure 9**). Clinically, findings from this study motivate the development of therapies focusing on key molecular targets involved in Ti-corrosion mediated failures and/or in the biological phenomenon underlying successful Ti-mediated osseointegration. Finally, it is important to consider that the present study describes a model to reproduce surface alterations observed in Ti-based devices retrieved from *in vivo* failures, in order to understand the host response to such alterations. Future studies are required to explore how challenging *in vivo* conditions (i.e., chronic inflammation and/or plaque accumulation) might in fact drive Ti corrosion *in vivo*.

DATA AVAILABILITY STATEMENT

The raw data supporting the conclusions of this article will be made available by the authors, without undue reservation.

ETHICS STATEMENT

The animal study was reviewed and approved by Institutional Committee for Animal Care and Use, School of Dentistry of Bauru, University of Sao Paulo, CEEPA-FOB/USP, #012/2014.

AUTHOR CONTRIBUTIONS

CB and GG contributed to the conception and design, the acquisition, analysis, and interpretation, drafted the manuscript, critically revised the manuscript, gave final approval, and agreed to be accountable for all aspects of work. FC, AF, AT, RT, RS contributed to the acquisition, analysis, and interpretation, gave final approval, and agreed to be accountable for all aspects of work. WF, SW, DS, and DR contributed to the acquisition, analysis, and interpretation, critically revised the manuscript, gave final approval, and agreed to be accountable for all aspects of work.

FUNDING

This work was supported by Grants from Fundação de Amparo à Pesquisa do Estado de São Paulo—FAPESP #2014/09590-8, #2015/18162-2, and #2015/24637-3, CNPq and CAPES. DR is supported from the National Institutes of Health (NIH R01 DE026736).

ACKNOWLEDGMENTS

The authors would like to thank Patrícia Germino and Danielli Ceolin from University of São Paulo–FOB/USP for their histological processing services.

SUPPLEMENTARY MATERIAL

The Supplementary Material for this article can be found online at: https://www.frontiersin.org/articles/10.3389/fmats.2021.651970/full#supplementary-material

REFERENCES

Albertini, M., Fernandez-Yague, M., Lazaro, P., Herrero-Climent, M., Rios-Santos, J., Bullon, P., et al. (2015). Advances in Surfaces and Osseointegration in Implantology. Biomimetic Surfaces. *Med. Oral* 20 (3), e316–e325. doi:10.4317/medoral.20353

Albrektsson, T., Chrcanovic, B., Jacobsson, M., and Wennerberg, A. (2017). Osseointegration of Implants—A Biological and Clinical Overview. *JSM Dent Surg.* 2 (3), 1022. doi:10.1016/b978-0-12-813384-2.00002-3

Albrektsson, T., Brånemark, P.-I., Hansson, H.-A., Kasemo, B., Larsson, K., Lundström, I., et al. (1983). The Interface Zone of Inorganic implantsIn Vivo: Titanium Implants in Bone. *Ann. Biomed. Eng.* 11 (1), 1–27. doi:10.1007/bf02363944

Albrektsson, T., Brånemark, P.-I., Hansson, H.-A., and Lindström, J. (1981). Osseointegrated Titanium Implants:Requirements for Ensuring a Long-Lasting, Direct Bone-To-Implant Anchorage in Man. *Acta Orthopaedica Scand.* 52 (2), 155–170. doi:10.3109/17453678108991776

Arteaga, A., Qu, J., Haynes, S., Webb, B. G., LaFontaine, J., and Rodrigues, D. C. (2021). Diabetes as a Risk Factor for Orthopedic Implant Surface Performance: A Retrieval and *In Vitro* Study. *J. Bio- Tribo-corrosion* 7 (2), 1–15. doi:10.1007/s40735-021-00486-8

Asri, R. I. M., Harun, W. S. W., Samykano, M., Lah, N. A. C., Ghani, S. A. C., Tarlochan, F., et al. (2017). Corrosion and Surface Modification on Biocompatible Metals: A Review. *Mater. Sci. Eng. C* 77, 1261–1274. doi:10.1016/j.msec.2017.04.102

Biguetti, C. C., Cavalla, F., Silveira, E. V., Tabanez, A. P., Francisconi, C. F., Taga, R., et al. (2019). HGMB1 and RAGE as Essential Components of Ti Osseointegration Process in Mice. *Front. Immunol.* 10, 709. doi:10.3389/fimmu.2019.00709

Biguetti, C. C., Cavalla, F., Silveira, E. M., Fonseca, A. C., Vieira, A. E., Tabanez, A. P., et al. (2018). Oral Implant Osseointegration Model in C57Bl/6 Mice: Microtomographic, Histological, Histomorphometric and Molecular Characterization. *J. Appl. Oral Sci.* 26, e20170601–24. doi:10.1590/1678-7757-2017-0601

Biguetti, C. C., Vieira, A. E., Cavalla, F., Fonseca, A. C., Colavite, P. M., Silva, R. M., et al. (2018). CCR2 Contributes to F4/80+ Cells Migration along Intramembranous Bone Healing in Maxilla, but its Deficiency Does Not Critically Affect the Healing Outcome. *Front. Immunol.* 9, 1804. doi:10.3389/fimmu.2018.01804 Available at: http://www.ncbi.nlm.nih.gov/pubmed/30147688

Cadosch, D., Chan, E., Gautschi, O. P., and Filgueira, L. (2009). Metal Is Not Inert: Role of Metal Ions Released by Biocorrosion in Aseptic Loosening-Current Concepts. *J. Biomed. Mater. Res.* 91A (4), 1252–1262. doi:10.1002/jbm.a.32625 Available at: http://www.ncbi.nlm.nih.gov/pubmed/19839047

Chandar, S., Kotian, R., Madhyastha, P., Kabekkodu, S. P., and Rao, P. (2017). *In vitro* evaluation of Cytotoxicity and Corrosion Behavior of Commercially Pure Titanium and Ti-6Al-4V Alloy for Dental Implants. *J. Indian Prosthodont. Soc.* 17 (1), 35–40. doi:10.4103/0972-4052.197936 Available at: http://www.ncbi.nlm.nih.gov/pubmed/28216843

Daubert, D. M., Pozhitkov, A. E., Safioti, L. M., and Kotsakis, G. A. (2019). Association of Global DNA Methylation to Titanium and Peri-Implantitis: A Case-Control Study. *JDR Clin Transl Res.* 4 (3), 284–291. doi:10.1177/2380084418822831

Davies, J. E. (2003). Understanding Peri-Implant Endosseous Healing. *J. Dental Educ.* 67 (8), 932–949. doi:10.1002/j.0022-0337.2003.67.8.tb03681.x Available at: http://www.ncbi.nlm.nih.gov/pubmed/12959168

Delgado-Ruiz, R., and Romanos, G. (2018). Potential Causes of Titanium Particle and Ion Release in Implant Dentistry: A Systematic Review. *Int. J. Mol. Sci. MDPI AG* 19, 119. doi:10.3390/ijms19113585 Available at: http://pmc/articles/PMC6274707/

Dini, C., Costa, R. C., Sukotjo, C., Takoudis, C. G., Mathew, M. T., and Barão, V. A. R. (2020). Progression of Bio-Tribocorrosion in Implant Dentistry. *Front. Mech. Eng.* 6 (1), 1. doi:10.3389/fmech.2020.00001 Available at: www.frontiersin.org

Donath, K., Laaß, M., and Günzl, H. J. (1992). The Histopathology of Different Foreign-Body Reactions in Oral Soft Tissue and Bone Tissue. *Virchows Arch. A. Pathol. Anat. Histopathol* 420 (2), 131–137. doi:10.1007/bf02358804

Flatebø, R. S., Johannessen, A. C., Grønningsæter, A. G., Bøe, O. E., Gjerdet, N. R., Grung, B., et al. (2006). Host Response to Titanium Dental Implant Placement Evaluated in a Human Oral Model. *J. Periodontol.* 77 (7), 1201–1210. doi:10.1902/jop.2006.050406

Gindri, I. M., Siddiqui, D. A., Frizzo, C. P., Martins, M. A. P., and Rodrigues, D. C. (2015). Ionic Liquid Coatings for Titanium Surfaces: Effect of IL Structure on Coating Profile. *ACS Appl. Mater. Inter.* 7 (49), 27421–27431. doi:10.1021/acsami.5b09309 Available at: http://www.ncbi.nlm.nih.gov/pubmed/26594841

Gomes, A. M., Douglas-de-Oliveira, D. W., Ferreira, S. D., Silva, T. A. D., Cota, L. O. M., and Costa, F. O. (2019). Periodontal Disease, Peri-Implant Disease and Levels of Salivary Biomarkers IL-1beta, IL-10, RANK, OPG, MMP-2, TGF-Beta and TNF-Alpha: Follow-Up over 5 Years. *J. Appl. Oral Sci.* 27, e20180316. doi:10.1590/1678-7757-2018-0316 Available at: http://www.ncbi.nlm.nih.gov/pubmed/30810638

Haleem-Smith, H., Argintar, E., Bush, C., Hampton, D., Postma, W. F., Chen, F. H., et al. (2012). Biological Responses of Human Mesenchymal Stem Cells to Titanium Wear Debris Particles. *J. Orthop. Res.* 30 (6), 853–863. doi:10.1002/jor.22002 Available at: http://www.ncbi.nlm.nih.gov/pubmed/22083964

Hallab, N. J., and Jacobs, J. J. (2017). Chemokines Associated with Pathologic Responses to Orthopedic Implant Debris. *Front. Endocrinol.* 8, 5. doi:10.3389/fendo.2017.00005 Available at: http://www.ncbi.nlm.nih.gov/pubmed/28154552

Hanawa, T. (2019). Titanium-Tissue Interface Reaction and its Control with Surface Treatment. *Front. Bioeng. Biotechnol.*7, 170. doi:10.3389/fbioe.2019.00170 Available at: http://www.ncbi.nlm.nih.gov/pubmed/31380361

Hernigou, P., Intrator, L., Bahrami, T., Bensussan, A., and Farcet, J. P. (1999). Interleukin-6 in the Blood of Patients with Total Hip Arthroplasty without Loosening. *Clin. Orthop. Relat. Res.* 18, 366147–366154. doi:10.1097/00003086-199909000-00018 Available at: http://www.ncbi.nlm.nih.gov/pubmed/10627728

Institute of Laboratory Animal Resources (U.S.) (2011). *Committee on Care and Use of Laboratory Animals. Guide for the Care and Use of Laboratory Animals*. Bethesda, MD: NIH publication, U.S. Dept. of Health and Human Services, Public Health Service; p. v.

Jain, S. S., Schramm, S. T. J., Siddiqui, D. A., Huo, W., Palmer, K. L., Wilson, T. G., et al. (2020). Effects of Multiple Implantations of Titanium Healing Abutments: Surface Characteristics and Microbial Colonization. *Dental Mater.* 36 (9), e279–e291. doi:10.1016/j.dental.2020.05.016

Lakkasetter Chandrashekar, B., Siddiqui, D. A., Palmer, K. L., and Rodrigues D, C. (2021). Titanium Surfaces and Detoxification Procedures: Effects of Bacterial Biofilm and Citric Acid Exposure on Oxide Layer Behavior. *J. Bio- Tribo-corrosion* 7 (2), 1–13. doi:10.1007/s40735-021-00484-w

Lausmaa, J., and Linder, L. (1988). Surface Spectroscopic Characterization of Titanium Implants after Separation from Plastic-Embedded Tissue. *Biomaterials* 9 (3), 277–280. doi:10.1016/0142-9612(88)90098-1 Available at: http://www.ncbi.nlm.nih.gov/pubmed/3408802

Lin, Z., Rios, H. F., Volk, S. L., Sugai, J. V., Jin, Q., and Giannobile, W. V. (2011). Gene Expression Dynamics during Bone Healing and Osseointegration. *J. Periodontol.* 82 (7), 1007–1017. doi:10.1902/jop.2010.100577 Available at: http://www.ncbi.nlm.nih.gov/pubmed/21142982

Mariani, E., Lisignoli, G., Borzi, R. M., and Pulsatelli, L. (2019). Biomaterials: Foreign Bodies or Tuners for the Immune Response?. *Int. J. Mol. Sci.* 20 (3). doi:10.3390/ijms20030636 Available at: http://www.ncbi.nlm.nih.gov/pubmed/30717232

Messer, R. L., Seta, F., Mickalonis, J., Brown, Y., Lewis, J. B., and Wataha, J. C. (2010). Corrosion of Phosphate-Enriched Titanium Oxide Surface Dental Implants (TiUnite) under In Vitro Inflammatory and Hyperglycemic Conditions. *J. Biomed. Mater. Res. B Appl. Biomater.* 92 (2), 525–534. doi:10.1002/jbm.b.31548 Available at: http://www.ncbi.nlm.nih.gov/pubmed/20024965

Messer, R. L. W., Tackas, G., Mickalonis, J., Brown, Y., Lewis, J. B., and Wataha, J. C. (2009). Corrosion of Machined Titanium Dental Implants under Inflammatory Conditions. *J. Biomed. Mater. Res.* 88B (2), 474–481. doi:10.1002/jbm.b.31162

Mombelli, A., Hashim, D., and Cionca, N. (2018). What Is the Impact of Titanium Particles and Biocorrosion on Implant Survival and Complications? A Critical Review. *Clin. Oral Implants Res.* 29, 37–53. Available at: https://onlinelibrary.wiley.com/doi/full/10.1111/clr.13305

Mouhyi, J., Dohan Ehrenfest, D. M., and Albrektsson, T. (2012). The Peri-Implantitis: Implant Surfaces, Microstructure, and Physicochemical Aspects. *Clin. Implant Dent Relat. Res.*14 (2), 170–183. doi:10.1111/j.1708-8208.2009.00244.x Available at: http://www.ncbi.nlm.nih.gov/pubmed/19843108

Mouraret, S., Hunter, D. J., Bardet, C., Brunski, J. B., Bouchard, P., and Helms, J. A. (2014). A Pre-clinical Murine Model of Oral Implant osseointegrationA Pre-clinical Murine Model of Oral Implant Osseointegration. *BoneBone* 58, 177–184. doi:10.1016/j.bone.2013.07.021 Available at: http://www.ncbi.nlm.nih.gov/pubmed/23886841

Niinomi, M. (2008). Mechanical Biocompatibilities of Titanium Alloys for Biomedical Applications. *J. Mech. Behav. Biomed. Mater.* 1 (1), 30–42. doi:10.1016/j.jmbbm.2007.07.001 Available at: http://www.ncbi.nlm.nih.gov/pubmed/19627769

Niinomi, M., Liu, Y., Nakai, M., Liu, H., and Li, H. (2016). Biomedical Titanium Alloys with Young's Moduli Close to that of Cortical Bone. *Regen. Biomater.* 3 (3), 173–185. doi:10.1093/rb/rbw016 Available at: http://www.ncbi.nlm.nih.gov/pubmed/27252887

Noronha Oliveira, M., Schunemann, W. V. H., Mathew, M. T., Henriques, B., Magini, R. S., Teughels, W., et al. (2018). Can Degradation Products Released from Dental Implants Affect Peri-implant Tissues?. *J. Periodontal Res.* 53 (1), 1–11. doi:10.1111/jre.12479

Noumbissi, S., Scarano, A., and Gupta, S. (2019). A Literature Review Study on Atomic Ions Dissolution of Titanium and its Alloys in Implant Dentistry. *Materials* 12 (3), 112. doi:10.3390/ma12030368 Available at: http://pmc/articles/PMC6384935/

Okazaki, Y., and Gotoh, E. (2005). Comparison of Metal Release from Various Metallic Biomaterials in vitroComparison of Metal Release from Various Metallic Biomaterials In Vitro. *Biomaterials* 26 (1), 11–21. doi:10.1016/j.biomaterials.2004.02.005 Available at: http://www.ncbi.nlm.nih.gov/pubmed/15193877

Olmedo, D. G., Paparella, M. L., Spielberg, M., Brandizzi, D., Guglielmotti, M. B., and Cabrini, R. L. (2012). Oral Mucosa Tissue Response to Titanium Cover Screws. *J. Periodontol.* 83 (8), 973–980. doi:10.1902/jop.2011.110392

Olmedo, D. G., Tasat, D., Guglielmotti, M. B., and Cabrini, R. L. (2004). "Systemic and Local Tissue Response to Titanium Corrosion," in Transactions—7th World Biomaterials Congress, 1334.

Olmedo, D. G., Duffó, G., Cabrini, R. L., and Guglielmotti, M. B. (2008). Local Effect of Titanium Implant Corrosion: an Experimental Study in Rats. *Int. J. Oral Maxillofac. Surg.* 37 (11), 1032–1038. doi:10.1016/j.ijom.2008.05.013 Available at: http://www.ncbi.nlm.nih.gov/pubmed/18602796

Pajarinen, J., Kouri, V.-P., Jämsen, E., Li, T.-F., Mandelin, J., and Konttinen, Y. T. (2013). The Response of Macrophages to Titanium Particles Is Determined by Macrophage Polarization. *Acta Biomater.* 9 (11), 9229–9240. doi:10.1016/j.actbio.2013.06.027 Available at: http://www.ncbi.nlm.nih.gov/pubmed/23827094

Penmetsa, S., Shah, R., Thomas, R., Kumar, A., Gayatri, P., and Mehta, D. (2017). Titanium Particles in Tissues from Peri-Implant Mucositis: An Exfoliative Cytology-Based Pilot Study. *J. Indian Soc. Periodontol.* 21 (3), 192–194. doi:10.4103/jisp.jisp_184_16 Available at: htpp://pmc/articles/PMC5803873/

Pettersson, M., Kelk, P., Belibasakis, G. N., Bylund, D., Molin Thorén, M., and Johansson, A. (2017). Titanium Ions Form Particles that Activate and Execute Interleukin-1β Release from Lipopolysaccharide-Primed Macrophages. *J. Periodontal Res.* 52 (1), 21–32. doi:10.1111/jre.12364

Ramesh, D., Sridhar, S., Siddiqui, D. A., Valderrama, P., and Rodrigues, D. C. (2017). Detoxification of Titanium Implant Surfaces: Evaluation of Surface Morphology and Bone-Forming Cell Compatibility. *J. Bio- Tribo-corrosion* 3 (4), 1–13. doi:10.1007/s40735-017-0111-2

Rodrigues, D. C., Urban, R. M., Jacobs, J. J., and Gilbert, J. L. (2009). In Vivosevere Corrosion and Hydrogen Embrittlement of Retrieved Modular Body Titanium Alloy Hip-Implants. *J. Biomed. Mater. Res. B Appl. Biomater.* 88B (1), 206–219. doi:10.1002/jbm.b.31171 Available at: http://www.ncbi.nlm.nih.gov/pubmed/18683224

Rodrigues, D., Valderrama, P., Wilson, T., Palmer, K., Thomas, A., Sridhar, S., et al. (2013). Titanium Corrosion Mechanisms in the Oral Environment: A Retrieval Study. *Materials* 6 (11), 5258–5274. doi:10.3390/ma6115258Available at: http://www.ncbi.nlm.nih.gov/pubmed/28788388

Saini, M., Singh, Y., Arora, P., Arora, V., and Jain, K. (2015). Implant Biomaterials: A Comprehensive Review. *World J. Clin. Cases* 3 (1), 52–57. doi:10.12998/wjcc.v3.i1.52 Available at: http://www.ncbi.nlm.nih.gov/pubmed/25610850

Shah, R., Penmetsa, D. S. L., Thomas, R., and Mehta, D. S. (2016). Titanium Corrosion: Implications for Dental Implants. *Eur. J. Prosthodont. Restor Dent* 24 (4), 171–180. doi:10.1922/EJPRD_1531Shah10 Available at: http://www.ncbi.nlm.nih.gov/pubmed/28510370

Soler, M. D., Hsu, S. M., Fares, C., Ren, F., Jenkins, R. J., Gonzaga, L., et al. (2020). Titanium Corrosion in Peri-Implantitis. *Materials (Basel)* 13, 1–11. doi:10.26226/morressier.5ac3832a2afeeb00097a3e26 Available at: http://pmc/articles/PMC7730765/

Souza, J. C. M., Barbosa, S. L., Ariza, E. A., Henriques, M., Teughels, W., Ponthiaux, P., et al. (2015). How Do Titanium and Ti6Al4V Corrode in Fluoridated Medium as Found in the Oral Cavity? an In Vitro Study. *Mater. Sci. Eng. C* 47, 384–393. doi:10.1016/j.msec.2014.11.055 Available at: https://pubmed.ncbi.nlm.nih.gov/25492211/

Sridhar, S., Abidi, Z., Wilson, T. G., Jr., Valderrama, P., Wadhwani, C., Palmer, K., et al. (2016). *In Vitro* Evaluation of the Effects of Multiple Oral Factors on Dental Implants Surfaces. *J. Oral Implant* 42 (3), 248–257. doi:10.1563/aaid-joi-d-15-00165 Available at: http://www.ncbi.nlm.nih.gov/pubmed/26829492In

Sridhar, S., Wang, F., Wilson, T. G., Valderrama, P., Palmer, K., and Rodrigues, D. C. (2018). Multifaceted Roles of Environmental Factors toward Dental Implant Performance: Observations from Clinical Retrievals and In Vitro Testing. *Dent Mater.* 34 (11), e265–79. doi:10.1016/j.dental.2018.08.299 Available at: https://pubmed.ncbi.nlm.nih.gov/30220507/

Sridhar, S., Wilson, T. G., Jr., Valderrama, P., Watkins-Curry, P., Chan, J. Y., and Rodrigues, D. C. (2016). *In Vitro* Evaluation of Titanium Exfoliation during Simulated Surgical Insertion of Dental Implants. *J. Oral Implant* 42 (1), 34–40. doi:10.1563/aaid-joi-d-14-00230 Available at: http://www.ncbi.nlm.nih.gov/pubmed/25785647 In

Sridharan, R., Cameron, A. R., Kelly, D. J., Kearney, C. J., and O'Brien, F. J. (2015). Biomaterial Based Modulation of Macrophage Polarization: a Review and Suggested Design Principles. *Mater. Today* 18 (6), 313–325. doi:10.1016/j.mattod.2015.01.019

Suska, F., Esposito, M., Gretzer, C., Källtorp, M., Tengvall, P., and Thomsen, P. (2003). IL-1alpha, IL-1beta and TNF-Alpha Secretion during In Vivo/Ex Vivo Cellular Interactions with Titanium and copperIL-1α, IL-1β and TNF-α Secretion during In Vivo/Ex Vivo Cellular Interactions with Titanium and Copper. *Biomaterials* 24 (3), 461–468. doi:10.1016/s0142-9612(02)00359-9 Available at: http://www.ncbi.nlm.nih.gov/pubmed/12423601

Tengvall, P., and Lundström, I. (1992). Physico-chemical Considerations of Titanium as a Biomaterial. *Clin. Mater.* 9 (2), 115–134. doi:10.1016/0267-6605(92)90056-y Available at: http://www.ncbi.nlm.nih.gov/pubmed/10171197

Tîlmaciu, C.-M., Mathieu, M., Lavigne, J.-P., Toupet, K., Guerrero, G., Ponche, A., et al. (2015). *In vitro* and In Vivo Characterization of Antibacterial Activity and Biocompatibility: a Study on Silver-Containing Phosphonate Monolayers on Titanium. *Acta Biomater.* 15, 266–277. doi:10.1016/j.actbio.2014.12.020 Available at: http://www.ncbi.nlm.nih.gov/pubmed/25562573

Trombone, A. P. F., Cavalla, F., Silveira, E. M. V., Andreo, C. B., Francisconi, C. F., Fonseca, A. C., et al. (2016). MMP1-1607 Polymorphism Increases the Risk for Periapical Lesion Development through the Upregulation MMP-1 Expression in Association with Pro-inflammatory Milieu Elements. *J. Appl. Oral Sci.* 24 (4), 366–375. doi:10.1590/1678-775720160112 Available at: http://www.ncbi.nlm.nih.gov/pubmed/27556208

Vieira, A. E., Repeke, C. E., Ferreira Junior Sde, B., Colavite, P. M., Biguetti, C. C., Oliveira, R. C., et al. (2015). Intramembranous Bone Healing Process Subsequent to Tooth Extraction in Mice: Micro-computed Tomography, Histomorphometric and Molecular Characterization. *PLoS One* 10 (5), e0128021. doi:10.1371/journal.pone.0128021 Available at: http://www.ncbi.nlm.nih.gov/pubmed/26023920

Wachi, T., Shuto, T., Shinohara, Y., Matono, Y., and Makihira, S. (2015). Release of Titanium Ions from an Implant Surface and Their Effect on Cytokine Production Related to Alveolar Bone resorptionRelease of Titanium Ions from an Implant Surface and Their Effect on Cytokine Production Related to Alveolar Bone Resorption. *Toxicology* 327, 1–9. doi:10.1016/j.tox.2014.10.016 Available at: http://www.ncbi.nlm.nih.gov/pubmed/25446332

Wainszelbaum, M. J., Proctor, B. M., Pontow, S. E., Stahl, P. D., and Barbieri, M. A. (2006). IL4/PGE2 Induction of an Enlarged Early Endosomal Compartment in Mouse Macrophages Is Rab5-dependent. *Exp. Cell Res.* 312 (12), 2238–2251. doi:10.1016/j.yexcr.2006.03.025

Wheelis, S. E., Biguetti, C. C., Natarajan, S., Arteaga, A., El Allami, J., Lakkasettar Chandrashekar, B., et al. (2021). Cellular and Molecular Dynamics during Early Oral Osseointegration: A Comprehensive Characterization in the Lewis Rat. *ACS Biomater. Sci. Eng.* 11, 27. doi:10.1021/acsbiomaterials.0c01420 Available at: https://pubs.acs.org/doi/10.1021/acsbiomaterials.0c01420

Wheelis, S. E., Biguetti, C. C., Natarajan, S., Guida, L., Hedden, B., Garlet, G. P., et al. (2020). Investigation of the Early Healing Response to Dicationic Imidazolium-Based Ionic Liquids: A Biocompatible Coating for Titanium Implants. *ACS Biomater. Sci. Eng.* 6 (2), 984–994. doi:10.1021/acsbiomaterials.9b01884

Wheelis, S. E., Gindri, I. M., Valderrama, P., Wilson, T. G., Huang, J., and Rodrigues, D. C. (2016). Effects of Decontamination Solutions on the Surface of Titanium: Investigation of Surface Morphology, Composition, and Roughness. *Clin. Oral Implants Res.* 27 (3), 329–340. doi:10.1111/clr.12545 Available at: https://pubmed.ncbi.nlm.nih.gov/25580643/

Wheelis, S. E., Wilson, T. G., Valderrama, P., and Rodrigues, D. C. (2018). Surface Characterization of Titanium Implant Healing Abutments before and after Placement. *Clin. Implant Dent Relat. Res.* 20 (2), 180–190. doi:10.1111/cid.12566 Available at: https://pubmed.ncbi.nlm.nih.gov/29214721/

Conflict of Interest: The authors declare that the research was conducted in the absence of any commercial or financial relationships that could be construed as a potential conflict of interest.